University of Nevada, Reno

Violation of parity and time-reversal in atoms and molecules

A dissertation submitted in partial fulfillment of the requirements for the degree of Doctor of Philosophy in Physics

by

Boris Ravaine

Dr. Andrei Derevianko/Dissertation Advisor

May 2007

University of Nevada, Reno
Statewide · Worldwide

THE GRADUATE SCHOOL

We recommend that the dissertation
prepared under our supervision by

BORIS RAVAINE

Entitled

Violation Of Parity And Time-Reversal In Atoms And Molecules

be accepted in partial fulfillment of the
requirements for the degree of

DOCTOR OF PHILOSOPHY

Andrei Derevianko, Advisor

Peter Winkler, Committee Member

Alla Safronova, Committee Member

Bruce Blackadar, Committee Member

Hyung-June Woo, Graduate School Representative

Marsha H. Read, Ph. D., Associate Dean, Graduate School

May, 2007

Abstract

Symmetries of the Universe have always provided theoreticians with a powerful tool in their efforts to understand and unify physics laws. Three of them have shaped physics over the last 50 years: parity (P), charge conjugation (C), and time-reversal (T). Today, T-violation remains the most mysterious symmetry violation as it is not understood properly and as much stronger T-violating mechanisms are required to explain the matter-antimatter in the Universe. T-violation could be potentially observed in some recently proposed and on-going experiments with atoms and molecules. In particular, T-violation could manifest itself in electric dipole moment (EDM) elemetary particles and atoms.

Here I present results of three calculations in support of emerging searches for T violation:

1) A recently proposed experiment with liquid Xe at Princeton may significantly improve present limits on atomic EDM. We find that the liquid phase reduces the T-violating signal by only 40% still offering an improvement of several orders of magnitude to present limits for several sources of T-violation.

2) To guide emerging searches for electron EDMs with molecular ions, we estimate the EDM-induced energy corrections for hydrogen halide ions HBr^+ and HI^+. We find that the EDM-signal for the two ions differ by an unexpectedly large factor of fifteen due to a dissimilarity in the nature of the chemical bond. We conclude HI^+ ion may be a potentially competitive candidate for the EDM search. These observations provide guidelines for finding a even better molecular ion candidate.

3) T-violation in an atom leads to the T-odd polarizability $\beta^{\rm CP}$: a magnetic moment $\mu^{\rm CP}$ is induced by an electric field $\mathcal{E}_0$ applied to an atom, $\mu^{\rm CP} = \beta^{\rm CP}\mathcal{E}_0$. We estimate the T-violating polarizability for rare-gas atoms He through Rn. Finally, we evaluate a feasibility of setting a limit on electron EDM by measuring $\mu^{\rm CP}$ of liquid Xe. We find that such an

experiment could provide competitive bounds on electron EDM only if the present level of experimental sensitivity to ultra-weak magnetic fields is improved by several orders of magnitude.

Acknowledgments

I would like to sincerely thank the faculty and staff in the Department of Physics for everything they have taught me and for giving me the opportunity to complete my PhD. Misha Kozlov and Walter Johnson who gave me useful comments and suggestions when I had the chance to meet them. And of course my advisor who has been very patient with me providing me with the opportunity to work with him on his research project.

Contents

I. Introduction 1

A. Symmetries conservation and violation 1

1. General discussion 1

2. Symmetry violation 3

3. C,P and T violations 3

4. Elementary-particle models 4

B. Permanent electric-dipole moment (EDM) 4

1. Definition of an electric dipole moment 5

2. Why does an EDM violate both T and P symmetries? 5

3. How do EDM's predictions depend on the elementary-particle model? 7

C. My work 9

D. The proposed experiments 12

II. Effects of confinement on permanent electric-dipole moment of Xe atoms in liquid Xe 14

A. Introduction 14

B. Sources of atomic EDM 15

C. Cell model of liquid xenon 17

D. Atom in a cavity: DHF and RRPA solutions 19

E. Results for an isolated Xe atom 21

F. Influence of the cavity radius on the EDM 22

G. Different models for $R_{\rm cav}$ 23

H. Conclusion 25

III. Marked influence of the nature of chemical bond on CP-violating signature in molecular ions HBr^+ and HI^+ 26

A. Introduction 26

B. Molecular structure and EDM-induced corrections 28

C. Chemical bond 29

D. Ionic bond approximation for the HBr^+ ion 30

E. Covalent bond approximation for HI^+ 33

F. Conclusions 34

IV. T-odd polarizability of Xe atom in liquid Xe 36

A. Introduction 36

B. Formalism 38

1. Third-order formula for the induced magnetic moment 38

2. Dirac-Hartree-Fock approximation 39

C. Results for rare-gas atoms 41

1. Z^5 scaling and relation between EDM and NC contributions 42

D. Limits on electron EDM from measurement of T-odd polarizability 45

E. Conclusion 47

V. Conclusion 48

A. Relativistic atomic orbitals 50

B. Hartree-Fock approximation 52

C. Atomic Units 54

D. Sources of T violation in atoms 55

1. Electron EDM 55

2. Nuclear Schiff moment 55

3. T-odd semileptonic interaction 56

4. T-odd weak neutral current 56

E. Reduced Matrix elements 57

F. Derivation of Eq.(31) 58

G. Derivation of Eq.(32) 59

References 61

I. INTRODUCTION

A. Symmetries conservation and violation

1. General discussion

Since the beginning of physics, studying symmetries has provided theoreticians with an extremely powerful and useful tool in their effort to understand Nature. Little by little symmetries have become the backbone of our theoretical formulation of physical laws. In this section I give a short review of these symmetries.

If a symmetry is exact, i.e. not violated or broken by Nature, the result of any experiment is invariant under the corresponding symmetry operation. There are four main groups of symmetries that are of fundamental importance in physics:

- Permutation symmetry: wave functions are symmetric under the permutation of two bosons, but antisymmetric under the permutation of two fermions.
- Continuous space-time symmetries: translations, rotations, etc.
- Discrete symmetries: space inversion P, time-reversal T, charge conjugation C, etc.
- Unitary symmetries: U_1-symmetries such as those related to conservation of charge, baryon number and lepton number for example. SU_2-symmetry (nucleon isospin). SU_3-symmetry (quark color) and other SU_n-symmetries.

Among these, the first two groups, together with some of the U_1-symmetries and SU_3-symmetry in the last group, are believed to be exact. All the remaining symmetries are broken.

The root of all symmetry principles lies in the assumption that it is impossible to observe certain basic quantities. Lee [1] calls these quantities non-observable quantities. For example, the absolute time can not be measured, as one always has to specify the origin $t = 0$ at a chosen time. According to Lee, time is an non-observable quantity. The physical laws must then be invariant under a time translation, which is equivalent to changing the

origin of time,

$$t \rightarrow t + \tau. \tag{1}$$

Invariance of physical laws under time translation results in the conservation of energy. In classical mechanics this direct relation between conserved quantities and symmetries has been elucidated by Noether [2]. Another example is spatial direction: by assuming the absolute spatial direction to be non-observable, one can derive rotational invariance and obtain the conservation law of angular momentum. Table I summarizes these fundamental aspects for some symmetry principles used in physics.

Non-observable quantities	Symmetry transformations	Conservation laws
Difference between identical particles	Permutation	Bosons and fermions statistics
Absolute spacial position	Space translation	Momentum
Absolute time	Time translation	Energy
Absolute spatial direction	Rotation	Angular momentum
Absolute velocity	Lorentz transformation	Special relativity
Absolute right (or left)	P: Parity transformation	Parity invariance
Absolute time direction	T: t ->-t	Time-reversal invariance
Absolute sign of electric charge	C: e -> -e	Charge conjugation invariance
Relative phase between states of charge Q	$\Phi \rightarrow \Phi \exp[iQ\theta]$	Charge
Relative phase between states of baryon number N	$\Phi \rightarrow \Phi \exp[iN\theta]$	Baryon number
Relative phase between syates of lepton number L	$\Phi \rightarrow \Phi \exp[iL\theta]$	Lepton number
Difference between different coherent mixture of proton p and neutron n	(p,n) -> U(p,n)	Isospin

TABLE I: Non-observables, symmetry transformations and conservation laws [1].

2. Symmetry violation

Since the validity of all symmetry principles rests on the theoretical hypothesis of non-observation, the violation of a symmetry arises whenever what was thought not to be an observable turns out to be actually observable. In this sense the discovery of symmetry violations is not surprising. Some non-observable quantities may indeed be due to deeper exact symmetries, but some may simply be due to the limitations of our present ability to measure some symmetry-violating signals. As we improve our experimental techniques, our domain of observation also enlarges.

3. C,P and T violations

The notable examples of discrete symmetry violations are:

- The asymmetry of physical laws under space inversion $\boldsymbol{r} \rightarrow -\boldsymbol{r}$, also called right-left mirror transformation and denoted P for Parity.
- Particle-antiparticle conjugation C.
- Time-reversal symmetry T: the laws of physics are slightly different when the time is running backwards.

The same symmetry principle applies to any of the bilinear products CP,PT,TC, etc. However, according to the so-called CPT theorem, the triple product CPT (or its permutations PTC, TCP...) does represent an exact symmetry. The CPT theorem (1955) is based on the Lorentz invariance and the assumption of locality. Considering CPT an exact symmetry, T violation is equivalent to CP violation and can be called either T or CP violation. P-violation was suggested in 1956 by Lee and Yang [3] and it was observed the next year in the β decay of ^{60}Co nuclei [4]. CP ($=T$)-violation was suggested in 1957 [5] and it was observed for the first time in 1964 in the decay of kaon particle [6]. In 2001, T-violation was again detected in neutral B-meson decays in the BaBar experiment at SLAC [7]. In my dissertation I studied T-violation in atomic systems. For each system (chapters 2,3 and 4), the T violating signals would also violate P. But since P violation is well understood,

it is the T violation that is presently of interest. Note that the P-violation without the T-violation has already been measured in atoms in 1978 [8]. Although the T-violation has already been observed in high energy experiments, it is still remains a mystery. The most important motivation for studying T violation is that its origin is not understood. Another important reason, as discussed in Section I C, is that by probing T-violation one can detect new physics beyond the Standard Model of elementary particles. Also, the present mechanism of T-violation does not account for the matter-antimatter asymmetry in our Universe. Sakharov [9] proposed that this asymmetry could have arisen from T violating interactions at an early stage of the Big Bang. It would have caused a slight predominance of matter over antimatter and allowed matter to survive the subsequent mutual annihilation of particles with antiparticles and thus formed the Universe as we know it.

4. Elementary-particle models

The present state of knowledge about particles and their interactions is called the Standard Model (SM) of elementary particles. But the SM is incomplete and does not address many fundamental questions, like the origin of T-violation. In the SM the only source of T-violation is introduced artificially in the Cabibbo-Kobayashi-Maskawa matrix by adding the so-called δ phase factor. Theoreticians try to solve the inconsistencies of the SM by extending the SM or inventing new models, such as the left-right symmetric models in which right-handed W and Z bosons are added to the usual particles of the SM, multi-Higgs models, in which Higgs bosonic fields are added to the SM, supersymmetry (SUSY), string theory, M-theories, etc. Below, I will focus on electric dipole moments (EDM) and argue that EDMs could place important constraints on these models.

B. Permanent electric-dipole moment (EDM)

As I mentioned above, a symmetry is linked to non-observable quantities. One of such quantities for T and P symmetries is EDM of particles. In other words, measuring the EDM of a particle is equivalent to observation of T-violation and P-violation. Purcell and

Ramsey first suggested to look for EDM of particles in 1950, although at that time T and P were not known as broken symmetries yet. Then it was proven that EDMs could not exist because they would violate parity. The search for particles EDM stopped; till P-violation was discovered. But then Landau [10] showed that EDMs were forbidden due to T conservation. In 1964, when the T-violation was discovered the searches for EDMs reappeared. Yet, we have never been able to observe an EDM. In this Section I introduce the concept of EDM of a particle and explain why an EDM violates time-reversal and parity symmetries.

1. Definition of an electric dipole moment

The electric dipole moment $\boldsymbol{d}$ of a localized charge density distribution $\rho(\boldsymbol{x})$ is

$$\boldsymbol{d} = \int \boldsymbol{x}\rho(\boldsymbol{x})d\boldsymbol{x}. \tag{2}$$

It is a vector. A particle does not need to be charged to have an EDM. For example, a charge q displaced from a charge $-q$ by a distance r creates an EDM $\boldsymbol{d} = q\boldsymbol{r}$. More generally, a particle does not need to have a size. In the case of a point-like particle, one talks about an intrinsic EDM. For example, the electron, which is believed to be a point-like particle, can still have an EDM.

We will use the definition (2) to compute atomic EDMs. But definition (2) does not work for an intrinsic EDM. In this case we need a more general definition:

$$d_i = -\frac{\partial E}{\partial \mathcal{E}_i}, \tag{3}$$

where E is the energy of the particle and $\mathcal{E}_i$ is the electric field exerted upon the particle. Definition (3) is also compelling experimentally: quantum-mechanically, one can measure the energy E, but can not directly probe the charge distribution $\rho(\boldsymbol{x})$.

2. Why does an EDM violate both T and P symmetries?

The proof that a non-vanishing EDM violates T and P is based upon realization that the EDM of a particle with a definite total angular momentum $\boldsymbol{J}$ lies along its total angular

momentum [10]:

$$\boldsymbol{d} = d\boldsymbol{J}. \tag{4}$$

Here are two different arguments in favor of Eq. (4) presented in the literature:

- A particle's EDM necessarily lies along its total angular momentum because all the components perpendicular to that axis would average to zero [11].

- In quantum mechanics, a system is characterized by the internal angular momentum $\boldsymbol{J}$, the only vector in the system. If we could specify a direction in addition to and independent of the angular momentum, additional quantum numbers would be required [12].

I prefer the following explanation: if a particle has a total angular momentum $\boldsymbol{J}$, then any rotation of the particle about $\boldsymbol{J}$ just multiplies its wave function by a phase factor (a scalar). It does not change the properties of the particle and in particular the direction of the EDM. As a consequence, the EDM direction has to be along the angular momentum.

Now let us prove that if the laws of physics are invariant under T or P then EDM necessarily vanishes. Considering a particle under the time reversal operation (see Figure 1), we observe that the angular momentum $\boldsymbol{J}$ is reversed while $\boldsymbol{d}$ is not affected. And under the P transformation, the angular momentum stays the same, while the EDM is reversed. As a result, one obtains $\boldsymbol{d} = -d\boldsymbol{J}$. If the laws of physics are invariant under P and T, then, by comparing with Eq.(4), we arrive at a contradictory requirement $d = -d$, i.e., the particle can not possess EDM.

Remark: degenerate atomic states can lead to an atomic EDM without T violation. Degenerate states are eigenstates of the Hamiltonian with the same energy. Consider two degenerate states $(n = 2, l = 0)$ and $(n = 2, l = 1, m = 0)$ of non-relativistic hydrogen artom. A linear combination of these two states would produce an atomic EDM. However, there is no paradox here, because the resulting state does not have a definite angular momentum.

What about polar molecules? They can have a measurable EDM. Does it mean we can measure T violation? Polar molecules can have an EDM when at "rest",i.e., when they

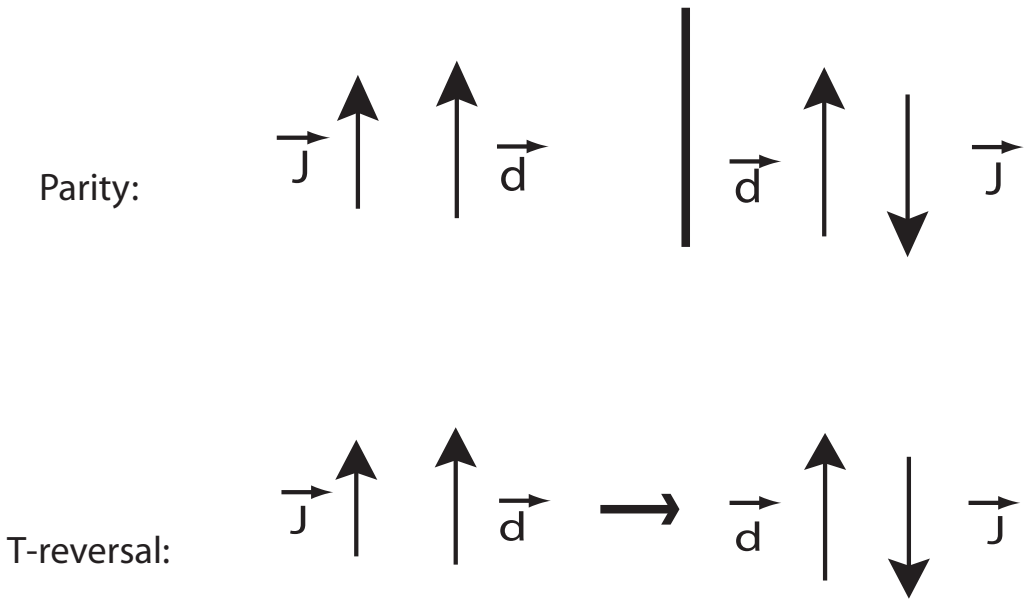

FIG. 1: Why does an EDM violate P and T?

don't have a definite angular momentum. Of course, a polar molecule can have a definite angular momentum, but then, such a rotating molecule does not have any EDM.

3. How do EDM's predictions depend on the elementary-particle model?

All models of elementary-particle predict EDMs for electrons, muons, neutrons, protons, nuclei and atoms. But these predictions depend greatly on the model. To illustrate that let us look at how one would compute an electron EDM. EDM can be observed when it interacts with an electric field (made of photons). So how does the T violation occur when a photon interacts with the electron? This interaction seems to respect T symmetry because the electromagnetic force conserves T and also because the Dirac equation is T invariant. The electron EDM arises indirectly since photons interact with other particles (quarks, W-bosons,...) and these particles in turn affect the electron. This process can involve T-violating weak interactions. At the end of the computation, one gets an energy E that depends on the direction of the electric field and thus the EDM, Eq.(3). Because other particles are involved in the computation of the electron EDM, the result depends on the model we use to describe various interactions. In the Standard Model (SM), the electron

EDM prediction is very smal, it can only originate from higher than three-loop diagrams. SM prediction for d_e is,

$$10^{-40} e\,\mathrm{cm} \leq |d_e(\mathrm{SM})| \leq 10^{-36} e\,\mathrm{cm}. \tag{5}$$

This prediction has to be compared with the present experimental limit obtained with thallium (Tl) atoms [13],

$$|d_e(\mathrm{Tl})| < 1.6 \times 10^{-27} e\,\mathrm{cm}. \tag{6}$$

As the reader can see, even with the best present experimental techniques, we are far from being able to measure an electron EDM in the range of predictions of the SM. An important point is that extensions to the SM generate EDMs that are comparable to the present limit. For example, if one complements the SM with the Higgs particles, then new possibilities are added for the T violation in the "Higgs sector". Dominant contributions for the electron EDM are given by diagrams such the one shown in Figure 2. The resulting limit on the electron EDM is increased to

$$10^{-29} e\,\mathrm{cm} \leq |d_e(\mathrm{SM} + \mathrm{Higgs})| \leq 10^{-25} e\,\mathrm{cm}, \tag{7}$$

and it is comparable to the present limit (6). More generally, predictions for the electron EDM from several competing models of elementary-particle physics are displayed in Figure 3 (taken from [13]). We observe that the upper limit on the electron EDM obtained in atomic experiments already put constraints on the parameters of supersymmetry (SUSY), Left-Right symmetric models in which right-handed W and Z bosons are added to the usual particles of the SM, and Multu-Higgs models in which the SM is complemented with Higgs particles. According to Khriplovich and Lamoreaux [12], searches for EDMs have ruled out most models suggested to explain T violation since its discovery. Electron EDM is not the only T-odd mechanism that depends greatly on different models of particle physics. Atomic physics experiments now, at our present level of accuracy, are extremely sensitive to possible new physics beyond the SM. Table II shows the constraints derived from atomic and molecular experiments on neutron, proton and electron EDMs.

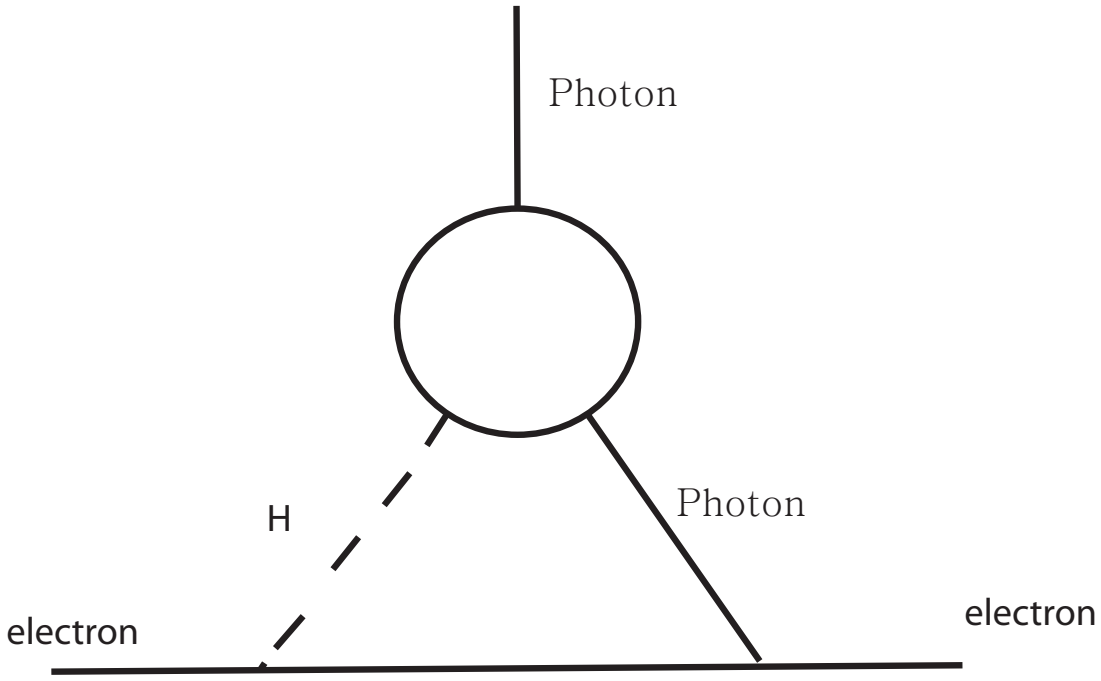

FIG. 2: Two-loop contribution to an electron EDM. A heavy particle (t-quark, W-boson or Higgs) is propagating in the upper loop [14].

Species examined	Species EDM	Derived EDM
Neutron	$< 6 \times 10^{-26} e\,\mathrm{cm}$	$d(\mathrm{neutron}) < 6 \times 10^{-26} e\,\mathrm{cm}$
^{199}Hg atom	$< 9 \times 10^{-28} e\,\mathrm{cm}$	$d(\mathrm{nucleus}) < 1 \times 10^{-24} e\,\mathrm{cm}$
TIF molecule	$< 6 \times 10^{-23} e\,\mathrm{cm}$	$d(\mathrm{proton}) < 6 \times 10^{-23} e\,\mathrm{cm}$
Thallium atom	$< 2 \times 10^{-24} e\,\mathrm{cm}$	$d(\mathrm{electron}) < 4 \times 10^{-27} e\,\mathrm{cm}$
YbF molecule	$< 4 \times 10^{-19} e\,\mathrm{cm}$	$d(\mathrm{electron}) < 4 \times 10^{-25} e\,\mathrm{cm}$

TABLE II: Upper limits on the measured species EDMs and the derived limits on particle EDMs (after [15]).

C. My work

Atoms amplify T-violating signals that occur at the fundamental level between elementary particles. Experimentalists exploit this amplification process by measuring a macroscopic T violating atomic signal. If we denote this signal as M, then M is related to the sources of T-violation by some structure factors. There are four main sources of T-violation

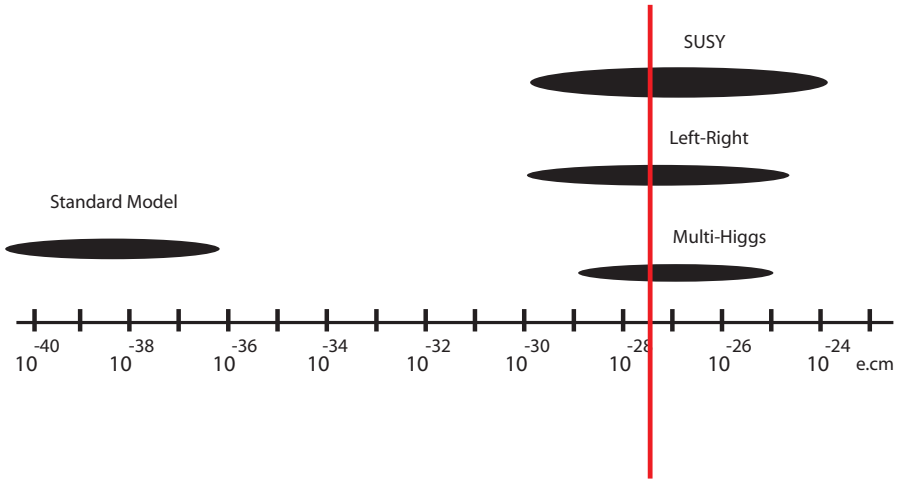

FIG. 3: Electron EDM (d_e) predictions from different models of particle physics. The vertical line corresponds to the present value of the best experimental limit on d_e [13].

in atoms and molecules:

- the EDM of the electron, d_e,
- the Schiff moment of the nucleus S [16],
- a semileptonic coupling constant, $C_{\rm TN}$,
- a weak neutral current constant, K.

The signal M can be parameterized as:

$$M = d_e F_e + S F_S + C_{\rm TN} F_C + K F_K, \tag{8}$$

where F_e, F_S, F_C and F_K are the structure factors. See Appendix D for more details about the atomic sources of T-violation. As discussed in Section I B 3, each model of elementary particles predicts different values of electron EDM, Schiff moment, semileptonic coupling constant, and weak neutral current constant. As a consequence, measuring T-violating

effects places important constraints on these models. Although these effects have not yet been found in atomic physics experiments, the limits set by measuring zero with a given precision have had decisive influences on elementary particle theories.

Atomic experiments probe particle physics in the "low-energy" domain, while particle accelerators directly test physics at high energy. These experiments are complementary. T-violating atomic experiments have been the subject of a program of ever increasing precision over the last 50 years and still further improvements are envisaged. They also present major interests in comparison to experiments carried out in particle accelerators: they are cheaper and can be built faster. They are called "table-top" experiments or "small-scale" experiment because they are done on an optical table.

The structure factors F_e, F_S, F_C, and F_K, multiplying T-violating parameters in Eq.(8) depend on the atomic or molecular properties. They can also be called enhancement factors because they amplify the small effects of T violation. My work was to compute these structure factors for three proposed experiments. So when experimental data are available, one can place constraints on the quantities d_e, S, C_{TN} and K, which can be interpreted in various models of particle physics (see Fig. 4).

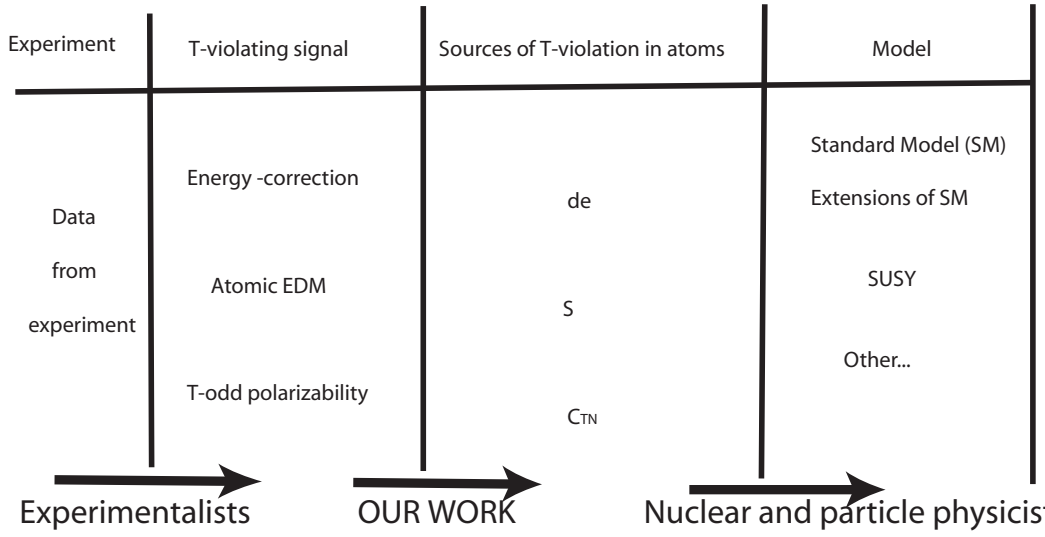

FIG. 4: Once experimentalists measure T-violating signals, we can constrain sources of T-violation and then nuclear and particle physicists can put limits on parameters of the different models of particle physics.

I worked on three different calculations of the structure factors. The following general scheme was applied:

(i) As every experiment is uniquely sensitive to the sources of T violation in atoms we had to decide which one would contribute the most to the experimental signal.

(ii) The second step consisted of deriving atomic-structure equations that link the sources to the T-odd experimental signal. It was important to use a relativistic description of the electron, i.e.,the four-component Dirac bi-spinor wave functions. We usually started with the Dirac-Hartree-Fock (DHF) solutions and then used more sophisticated many-body techniques. We simplified the equations by carrying out an angular momentum reduction.

(iii) The last step was to code those equations and compute the signal as a function of the T-odd sources.

D. The proposed experiments

Each chapter of the dissertation is devoted to a separate calculation.

1) The first calculation (Chapter 2) was in support of an experiment proposed by Romalis and Ledbetter [17] at Princeton University. They proposed to measure the EDM of xenon atoms in a liquid Xe sample. This experiment is expected to have several-order of magnitude improvement in sensitivity to many sources of T violation. The sources we took into account were: the nuclear Schiff moment, S, and the semileptonic T-odd interactions, C_{TN} **??**. To the best of my knowledge, the effect of the liquid environment on the atomic EDM has not been addressed previously.

2) The second experiment was proposed by R. Stutz and E. Cornell [18] at the University of Colorado, Boulder. They proposed to measure energy corrections due to the electron EDM in molecular ions. We were the first to calculate T-violation effects in such systems **??**. Here it was important to provide qualitative guidelines for emerging electron EDM search with molecular ions.

3) T-violation leads to magnetization of a sample placed in an electric field **??**. This could be interpreted as a T-odd polarization of an individual atom or molecule. We investigated this novel polarizability and related it to the electron EDM. Also we evaluated a

feasibility of using liquid Xe as the medium for measuring the T-violating polarizability **??**. As Baryshevsky recently pointed out **??** T-violating magnetization would also exists for a diamagnetic atom.

The common goal of all these experiments is to set constraints of T-violating EDMs probing new physics beyond the Standard Model of elementary particles.

II. EFFECTS OF CONFINEMENT ON PERMANENT ELECTRIC-DIPOLE MOMENT OF XE ATOMS IN LIQUID XE

Romalis and Ledbetter [17] recently proposed to search for an EDM of ^{129}Xe atom in a sample of liquid Xe. A substantial, several orders of magnitude improvement in sensitivity to sources of T-violation is anticipated. The purpose of this chapter is to compute the atomic EDM of Xe and investigate the effect of the liquid on the EDM value. The chapter is organized as follows. In the introduction, I explain the motivation for this experiment and briefly describe our main findings. In section B, I describe the computations of an atomic EDM using the atomic wave function. Section C presents the so-called cell model employed in our simulation of xenon liquid environment. In section D, I explain how we solve the atomic-structure problem within the cell model. Results for an isolated atom are presented in section E. Then, the influence of the liquid confinement on those results is analyzed (section F) , and limitations of the employed model are discussed (section G). Finally, the conclusions are drawn in section H. Atomic units $|e| = \hbar = m_e = 4\pi\varepsilon_0 \equiv 1$ are used throughout (see Appendix C for more details on atomic units).

A. Introduction

The most accurate to date determination of atomic EDM was carried on with ^{199}Hg atoms [19] in a gas cell. It set limits on a number of important parameters: CP-violating QCD vacuum angle, quark chromo-EDMs, semileptonic T-violating parameters, and restricts parameter space for certain extensions to the standard model. Liquid ^{129}Xe experiment will probe similar parameters but with a much improved sensitivity. Compared to gas phase experiments [20], a drastically improved sensitivity with liquid experiments is mainly due to the higher number densities of the liquid phase (10^{22} atoms/cm^3 in our case).

The very use of the liquid phase raises questions about density-dependent factors which can influence the outcome and interpretation of the experiment. For example, an EDM experiment with a molecular liquid was proposed in Ref.[21]. The authors found an additional suppression of the EDM signal by a factor of a hundred due to a reduced population of

molecular rotational levels in liquid. Although the experiment with liquid Xe will be free from such an effect, it is clear that the effects of the liquid phase on atomic EDMs have to be investigated.

An EDM of an atom is related to a strength of a T-violating source via electronic-structure (enhancement or shielding) factors. For an isolated Xe atom such factors were computed previously: P,T-odd semileptonic interactions were considered by Mårtensson-Pendrill [22] and nuclear Schiff moment by Dzuba et al. [23]. Here we employ a simple cell model to study density dependence of the electronic-structure factors. Technically, we extend the previous atomic relativistic many-body calculations by confining a Xe atom to a spherically-symmetric cavity. In a non-polar liquid such as liquid Xe, this cavity roughly approximates an averaged interaction with the neighboring atoms. Imposing proper boundary conditions at the cavity radius, first we solve the Dirac-Hartree-Fock (DHF) equations and then employ the relativistic random-phase approximation (RRPA) to account for correlations. To the best of our knowledge, here we report the first *ab initio* relativistic calculations of properties of a liquid. We find that compared to the EDM of an isolated atom, the resulting EDM of an atom of liquid Xe is suppressed by about 40%. Thus if the experiment with liquid Xe is carried out with the anticipated sensitivity, we expect that the inferred constraints on possible sources of T-violation would be indeed several orders of magnitude better than the present limits.

B. Sources of atomic EDM

The main sources of T-violation in atoms and molecules are listed in Appendix D. In the present section we are only interested in the T-violating sources that can produce an atomic EDM to Xe atoms. As introduced in the previous chapter, an atomic EDM is the electric dipole moment of the electronic wave function $|\Psi_0\rangle$, including all electrons. If $\boldsymbol{D}$ is the electric dipole moment operator then the atomic EDM is:

$$\boldsymbol{d} = \langle\Psi_0|\boldsymbol{D}|\Psi_0\rangle. \tag{9}$$

In atomic units (Appendix C) $\boldsymbol{D}$ is expressed as:

$$\boldsymbol{D} = -\sum_i \boldsymbol{r}_i, \tag{10}$$

where the sum is over each electron. The conventional atomic Hamiltonian H_0 among other symmetries is invariant with respect to space-reflection (P) and time reversal (T). Mathematically, this property is written with the anticommutation equalities:$[H_0, P] = 0$ and $[H_0, T] = 0$. As discussed in the introductory chapter, if P and T symmetries are conserved there is no EDM. Therefore, on very general grounds, an expectation value of the electric dipole operator $\boldsymbol{D} = -\sum_i \boldsymbol{r}_i$ in a non-degenerate atomic state $|\Psi_0\rangle$ vanishes. The tiny T-violating interactions, here generically denoted as $H_{\rm CP} = \sum_i h_{\rm CP}(\mathbf{r}_i)$, break the symmetry of the atom and induce a correction to the electronic state $|\tilde{\Psi}\rangle = |\Psi_0\rangle + |\delta\Psi\rangle$. To the lowest order of perturbation theory

$$|\delta\Psi\rangle = \sum_k |\Psi_k\rangle \, \frac{\langle\Psi_k|H_{\rm CP}|\Psi_0\rangle}{E_0 - E_k}\,, \tag{11}$$

where E_k and $|\Psi_k\rangle$ are eigenvalues and eigenfunctions of H_0. Due to selection rules, the $|\delta\Psi\rangle$ admixture has a parity opposite to the one of the reference state $|\Psi_0\rangle$. Because of this opposite-parity admixture, the atom acquires a permanent EDM

$$\mathbf{d} = \langle\tilde{\Psi}|\mathbf{D}|\tilde{\Psi}\rangle = 2\langle\Psi_0|\mathbf{D}|\delta\Psi\rangle\,. \tag{12}$$

Now we specify particular forms of $H_{\rm CP}$. What sources are we going to choose? An analysis [12] shows that for diamagnetic atoms, such as Xe, the EDM predominantly arises due to P,T-odd semi-leptonic interaction $H_{\rm TN}$ between electrons and nucleons and also due to interaction $H_{\rm SM}$ of electrons with the so-called nuclear Schiff moment [16]. Smaller atomic EDM is generated by intrinsic EDM of electrons and we will not consider this mechanism here.

Explicitly, the effective P,T-odd semileptonic interaction Hamiltonian may be represented as [22]

$$h_{\rm TN}(\mathbf{r}_e) = \sqrt{2} G_{\rm F}\, C_{\rm TN}\, \boldsymbol{\sigma}_N \cdot \left(i\gamma_0\gamma_5\, \boldsymbol{\sigma}\right)_e \rho_N\left(\mathbf{r}_e\right)\,. \tag{13}$$

Here subscripts e and N distinguish between operators acting in the space of electronic and nuclear coordinates respectively. $C_{\rm TN}$ is the semi-leptonic coupling constant already

mentioned in the introductory chapter . Due to averaging over nuclear degrees of freedom, this interaction depends on nuclear density distribution $\rho_N(r)$. In the following, we approximate $\rho_N(r)$ as a Fermi distribution $\rho_N(r) = \rho_0/(1+\exp[(r-c)/a])$ with $c = 5.6315$ fm and $a = 0.52$ fm. Finally, $G_{\rm F} \approx 2.22254 \times 10^{-14}$ a.u. is the Fermi constant.

The interaction of an electron with the nuclear Schiff moment $\mathbf{S}$ has the form [24]

$$h_{\rm SM}(\mathbf{r}_e) = \frac{3}{B_4}\,\rho_N\left(\mathbf{r}_e\right)\left(\mathbf{r}_e\cdot\mathbf{S}\right)\,, \tag{14}$$

where $B_4 = \int_0^\infty r^4 \rho_N\left(r\right) dr$ is the fourth-order moment of the nuclear distribution. The Schiff moment characterizes a difference between charge and EDM distributions inside the nucleus (see Appendix D).

Finally, let us emphasize that both $h_{\rm TN}$ and $h_{\rm SM}$ are contact interactions. They occur when an electron penetrates the nucleus. The electron speed at the nucleus is approximately $\alpha Z c \simeq \frac{1}{2}c$ ($Z = 54$), i.e., a fully relativistic description of electronic motion is important in this problem.

C. Cell model of liquid xenon

Here we employ a simple cell model (see [25] and references therein) to estimate the effects of the environment on permanent EDM of a given atom. According to the cell model, we confine an atom to a spherical cavity of radius

$$R_{\rm cav} = \left(\frac{3}{4\pi}\,\frac{1}{n}\right)^{1/3}\,, \tag{15}$$

n being the number density of the sample. This comes from a simple model where atoms are like hard spheres as show in Figure 5.

For a density of liquid Xe of 500 amagat (amagat density unit is equal to 44.615 moles per cubic meter (mol/m^3)), $R_{\rm cav} \simeq 4.9$ bohr. In non-relativistic calculations periodicity requires that the normal component of the gradient of electronic wave-function vanishes at the surface of the cell (see, e.g., [26])

$$\frac{\partial\Psi}{\partial r}(R_{\rm cav}) = 0\,. \tag{16}$$

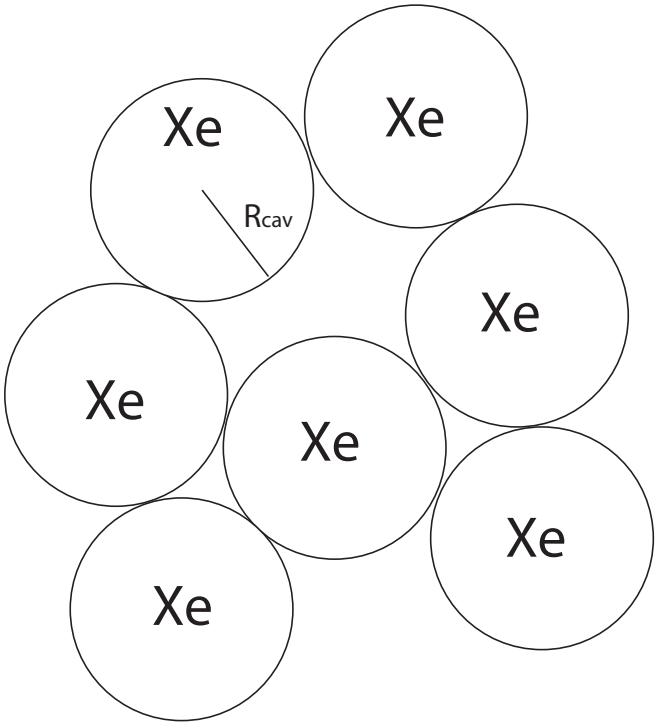

FIG. 5: Hard sphere model: Xe atoms in the liquid state are moving like hard spheres of radius $R_{\rm cav}$.

Before proceeding with a technical question of implementing these boundary conditions in relativistic calculations, we notice that the cell model implicitly incorporates an average polarization interaction with the media. Indeed, the Hamiltonian of an atom placed in the liquid in addition to the conventional atomic Hamiltonian H_0 includes interaction of electrons with the rest of the atoms in the media. This interaction is dominated by polarization potential. An important point is that the *averaged* polarization interaction can be expressed as $V_p = -1/2(1-\epsilon^{-1})R_{\rm cav}^{-1}$, where ϵ is the dielectric constant of the media [26]. This interaction does not depend on electronic coordinate — it is just an additive constant which does not affect calculations of EDM. Thus we may approximate the total Hamiltonian with the traditional atomic Hamiltonian H_0.

Further, the spherical symmetry of the cell allows us to employ traditional methods of atomic structure. The only modification is due to boundary conditions (16). However, in relativistic calculations, a special care should be taken when implementing this boundary

condition. Indeed, the Dirac bi-spinor may be represented as (Appendix A)

$$\varphi_{n\kappa m}(\mathbf{r}) = \frac{1}{r}\begin{pmatrix} P_{n\kappa}(r)\ \ \Omega_{\kappa m}(\widehat{\mathbf{r}}) \\ iQ_{n\kappa}(r)\ \ \Omega_{-\kappa m}(\widehat{\mathbf{r}}) \end{pmatrix}, \tag{17}$$

where P and Q are the large and small radial components respectively and Ω is the spherical spinor. The angular quantum number $\kappa = (l-j)\,(2j+1)$. The nonrelativistic boundary condition (16) applied directly to the above ansatz would lead to *two* separate constraints on P and Q. This over-specifies boundary conditions and leads to the Klein paradox.

A possible relativistic generalization of the boundary condition (16) is

$$\frac{d}{dr}\frac{P_{n\kappa}}{r}(R_{\rm cav}) = \frac{d}{dr}\frac{Q_{n\kappa}}{r}(R_{\rm cav})\,. \tag{18}$$

Since in the non-relativistic limit the small component Q vanishes, this generalization subsumes Eq. (16). Due to a semi-qualitative nature of our calculations, here we have chosen to use simpler (MIT bag model) boundary condition

$$P_{n\kappa}(R_{\rm cav}) = Q_{n\kappa}(R_{\rm cav})\,. \tag{19}$$

Non-relativistically it corresponds to impenetrable cavity surface. Compared to this condition, the periodic boundary conditions (18) are "softer", i.e., they modify the free-atom wavefunctions less significantly; we expect that our use of Eq. (19) would somewhat overestimate the effects of confinement in the liquid.

D. Atom in a cavity: DHF and RRPA solutions

To reiterate the discussion so far, within the cell model, the complex liquid-structure problem is reduced to solving atomic many-body Dirac equation with boundary conditions (19). The atomic-structure analysis is simplified by the fact that Xe is a closed-shell atom. Below I self-consistently solve the DHF equations inside the cavity. Then we employ more sophisticated RRPA. See Appendix B for a more detailed description of these two methods.

At the DHF level, the atomic wavefunction,Ψ_0, is represented by the Slater determinant of all occupied orbitals φ_a,

$$\Psi_0(\xi_1,\xi_2,...,\xi_N)=\frac{1}{\sqrt{N!}}\begin{vmatrix}\varphi_1(\xi_1) & \varphi_2(\xi_1) & ... & \varphi_N(\xi_1)\\ \varphi_1(\xi_2) & \varphi_2(\xi_2) & ... & \varphi_N(\xi_2)\\ \vdots & \vdots & & \vdots\\ \varphi_1(\xi_N) & \varphi_2(\xi_N) & ... & \varphi_N(\xi_N)\end{vmatrix}, \tag{20}$$

where a denotes a set of quantum numbers $n\kappa m$, N is the total number of electrons, and ξ_i encapsulates coordinate and spin degrees of freedom for the i^{th} electron. The Slater determinant is just the antisymmetric form of the many-electron wave function as required by the Pauli exclusion principle.

These orbitals are determined from a set of DHF equations

$$\left(c(\boldsymbol{\alpha}\cdot\mathbf{p})+\beta c^2+V_{\text{nuc}}+V_{\text{DHF}}\right)\varphi_a=\varepsilon_a\varphi_a\,, \tag{21}$$

where V_{nuc} is a potential of the Coulomb interaction with a finite-size nucleus of charge density $\rho_N(r)$ and V_{DHF} is non-local self-consistent DHF potential. The DHF potential depends on all the core orbitals. Similar equations may be written for virtual orbitals φ_m.

We solved the DHF equations in the cavity using a B-spline basis set technique by [27]. This technique is based on the Galerkin method: the DHF equations are expressed in terms of an extremum of an action integral S_A. The boundary conditions are incorporated in the S_A as well. Further, the action integral is expanded in terms of a finite set of basis functions (B-splines). Minimization of such S_A with respect to expansion coefficients reduces solving integro-differential DHF equations to solving symmetric generalized eigenvalue problem of linear algebra. The resulting set of basis functions is finite and can be considered as numerically complete. In a typical calculation we used a set of basis functions expanded over 100 B-splines.

Technically, we formed the initial DHF potential V_{DHF} using the DHF core orbitals for a free atom ($R_{\text{cav}}=\infty$). Then we solved the eigenvalue problem iteratively, at the beginning of each iteration assembling a new V_{DHF} from the core orbitals obtained at the previous iteration. The convergence was monitored by comparing relative changes in the energies of core orbitals at each iteration. As a result we obtained solutions of the DHF equations adjusted to the finite value of the cavity radius.

Given a numerically complete set of DHF eigenfunctions $\{\varphi_i\}$, the permanent atomic EDM, Eq.(12), may be expressed as

$$\mathbf{d}^{\rm DHF} = 2\sum_{m,a} \frac{\langle\varphi_a|\mathbf{r}|\varphi_m\rangle\langle\varphi_m|h_{\rm CP}|\varphi_a\rangle}{\varepsilon_m - \varepsilon_a}\,, \tag{22}$$

where a runs over occupied and m over virtual orbitals. Here $h_{\rm CP}$ is either a semileptonic interaction, Eq. (D4), or an interaction with the nuclear Schiff moment, Eq. (D3). An additional peculiarity related to the Dirac equation is an appearance of negative energy states ($\varepsilon_m < -m_e c^2$) in the summation over intermediate states in Eq. (22). We have verified that these states introduce a completely negligible correction to the computed EDMs.

To improve upon the DHF approximation, we have also computed EDMs using RRPA method (Appendix B). This approximation describes a dynamic linear response of an atom to a perturbing one-body interaction (e.g., $H_{\rm CP}$). The perturbation modifies core orbitals thus changing the DHF potential. This modification of $V_{\rm DHF}$ in turn requires the orbitals to adjust self-consistently. Such a readjustment process defines an infinite series of many-body diagrams, shown, e.g., in Ref.[22]. The RRPA series can be summed to all orders using iterative techniques or solving DHF-like equations. We used an alternative method of solutions based on the use of basis functions [27]. As an input, we used the DHF basis functions generated in the cavity (see discussion above), i.e. the boundary conditions were satisfied automatically. As a result of solving the RRPA equations, we have determined a quasi-complete set of particle-hole excited states and their energies. Then the EDMs are determined using expressions similar to Eq. (11) and (12).

E. Results for an isolated Xe atom

In this short section, I present the results of our calculations for an isolated atom ($R_{\rm cav} = \infty$) and compare them to previous results obtained by other groups. For the Schiff-moment-induced EDM, our results,

$$\begin{aligned} d_{\rm SM}^{\rm DHF} &= 2.88\left(\frac{S}{e\,\mathrm{fm}^3}\right)\times 10^{-18}\,e\,\mathrm{cm}, \\ d_{\rm SM}^{\rm RRPA} &= 3.78\left(\frac{S}{e\,\mathrm{fm}^3}\right)\times 10^{-18}\,e\,\mathrm{cm}\,, \end{aligned}$$

are in agreement with the recent calculations by Dzuba et al. [23] $\left(3.8\left(\frac{S}{e\,\mathrm{fm}^3}\right)\times 10^{-18}\,e\,\mathrm{cm}\right)$. For the EDM induced by T,P–odd semileptonic interactions we obtain

$$d_{\mathrm{TN}}^{\mathrm{DHF}} = 8.44\times 10^{-13}\; C_{\mathrm{TN}}\,\sigma_N\,\mathrm{a.u.}\,,$$
$$d_{\mathrm{TN}}^{\mathrm{RRPA}} = 10.7\times 10^{-13}\; C_{\mathrm{TN}}\,\sigma_N\,\mathrm{a.u.}.$$

These values are to be compared with the results by Mårtensson-Pendrill [22], $d_{\mathrm{TN}}^{\mathrm{DHF}} = 7.764$ and $d_{\mathrm{TN}}^{\mathrm{RRPA}} = 9.808$ in the same units. The reason for the 10% difference between our results and those from Ref. [22] is not clear.

F. Influence of the cavity radius on the EDM

Before presenting results for finite cavity radii, let us consider individual contributions to EDM from various shells of Xe atom. These contributions for the Schiff-moment-induced EDM of an isolated atom are listed in Table III. A similar table, but for the EDM arising from semileptonic interactions is given in Ref. [22]. From these tables we observe that the dominant contribution to EDMs comes from the outer $n = 5$ shell. Thus we anticipate that a noticeable density dependence should occur when R_{cav} becomes comparable to the size of external $n = 5$ shell. We also notice that the contribution from the outer shell is relatively more important in RRPA calculations than at the DHF level, i.e., the RRPA results should exhibit stronger density dependence.

These qualitative conclusions for a confined atom are supported by our numerical results, presented in Fig. 6. Here we plot the ratios of atomic EDMs for the confined and isolated atoms as a function of R_{cav}. The EDMs become smaller as the density increases, $n \propto R_{\mathrm{cav}}^{-3}$. At the density of liquid Xe, $R_{\mathrm{cav}} \approx 4.9$ bohr , the more accurate RRPA results show a 25% suppression of the atomic EDM due to confinement. Overall there is a noticeable density-dependence of atomic EDM. We expect the EDM signal (if found) to be broadened. The relevant characteristic width of the signal can be simply estimated from our Fig. 6 from the mean density fluctuations.

	DHF	RRPA
$n = 1$	0.039	0.039
$n = 2$	0.091	0.092
$n = 3$	0.20	0.21
$n = 4$	0.52	0.64
$n = 5$	2.0	2.8
Total	2.88	3.78

TABLE III: Individual contributions from various shells to the EDM of a free ^{129}Xe atom in the DHF and RRPA methods. The EDM is induced by the nuclear Schiff moment and it is given in units of $S/(e\,\mathrm{fm}^3) \times 10^{-18}\, e\,\mathrm{cm}$.

From Fig. 6 we notice that both semileptonic– and Schiff–moment–induced EDMs scale with R_{cav} in a similar fashion. This similarity can be explained from the following arguments. The values of CP-violating matrix elements, Eq.(D4) and Eq.(D3), are accumulated inside the nucleus. Non-relativistically, as $r \to 0$ the wavefunctions scale as $\varphi_{nlm}(\mathbf{r}) \approx N_{nl}(R_{\mathrm{cav}}) \times r^l Y_{lm}(\hat{\mathbf{r}})$, where N_{nl} are normalization factors. Therefore the dominant contribution to the EDM, Eq.(22) arises from mixing of s and p states. By factorizing the matrix element of h_{CP} as $\langle \varphi_{ns}|h_{\mathrm{CP}}|\varphi_{n'p}\rangle \approx N_{ns}(R_{\mathrm{cav}})N_{n'p}(R_{\mathrm{cav}}) \times \langle s|h_{\mathrm{CP}}|p\rangle$ we see that the R_{cav}–independent factor $\langle s|h_{\mathrm{CP}}|p\rangle$ can be pulled out of the summation over atomic orbitals in Eq.(22). Thus, both semileptonic– and Schiff–moment–induced EDMs exhibit approximately the same scaling with the cavity radius. A correction to this "similarity scaling law" may arise, for example, due to different selection rules involved for the two EDM operators.

G. Different models for R_{cav}

From Fig.6 we see that for small cavity radii (smaller than 6 bohr) the EDM depends greatly on R_{cav}. It seems worthwhile to try to improve upon our estimate for the cavity radius of the cell model, Eq.(15). According to Eq.(15), N atoms would occupy a volume equal N times the volume of one atom, $N\frac{4\pi}{3}(R_{\mathrm{cav}})^3$. This would hold only if empty spaces

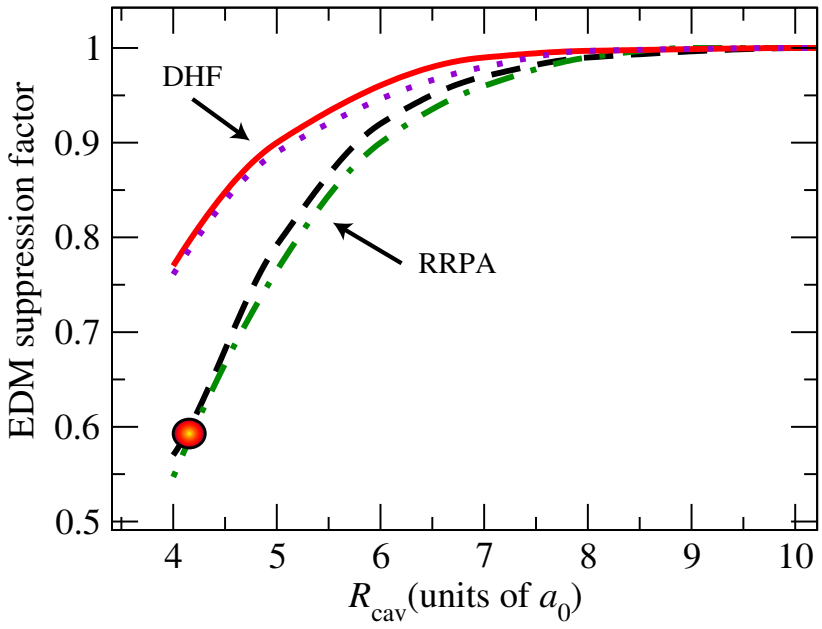

FIG. 6: The ratios of atomic EDMs for the confined and isolated atoms (suppression factor) as a function of cavity radius. The upper and lower sets of two curves are obtained with the DHF and RRPA methods respectively. EDMs induced by P,T–odd semileptonic interactions are shown as solid and dashed lines, while EDMs due to the Schiff moment — as dotted and dashed-dotted lines. Heavy dot marks our final results for liquid Xe.

between the hard spheres were discarded. A better estimate for $R_{\rm cav}$ can be obtained by noticing that a dense liquid may be considered as a solid with vacancies. It means that the cavity radius $R_{\rm cav}$ has to be computed with the solid number density n_S using Xe solid structure. Xe condenses into face-centered cubic structure. The first nearest-neighbor shell contains twelve atoms (partially justifying the spherical symmetry of the elementary cell). The formula that links $R_{\rm cav}$ to n_S is:

$$R_{\rm cav} = \left(\frac{5}{16\sqrt{2}n_S}\right)^{\frac{1}{3}}. \tag{23}$$

The density of the solid Xe is $\rho_S = 3.54$ g/cm^3, implying the half-radius of this shell of 4.2 bohr, somewhat smaller than $R_{\rm cav} \approx 4.9$ bohr of the liquid cell model, Eq.(15). As follows from Fig. 6, this difference leads to more pronounced suppression of the atomic EDM by 40%.

H. Conclusion

To reiterate, our work was motivated by anticipated significant improvements in sensitivity to atomic EDMs in experiments with liquid ^{129}Xe [17]. We investigated confining effects of the environment on the EDM of Xe atom. We carried out the analysis in the framework of the cell model coupled with relativistic atomic-structure calculations. We found that compared to an isolated atom, the EDM of an atom of liquid Xe is reduced by about 40%. Thus if the experiment with liquid Xe is carried out with the anticipated sensitivity, we expect that the inferred constraints on possible sources of CP-violation would be indeed several orders of magnitude better than the present limits.

III. MARKED INFLUENCE OF THE NATURE OF CHEMICAL BOND ON CP-VIOLATING SIGNATURE IN MOLECULAR IONS HBr^+ AND HI^+

Stutz and Cornell from the University of Colorado, Boulder, proposed to use molecular ions to measure the electron EDM [18]. In this new chapter, the source of T-violation involved is the electron EDM. A source that the previous experiment (Chapter II) was not sensitive to. Contrary to the liquid xenon experiment, where the atomic EDM could be measured almost directly via spin precession, electron EDM can not be measured in the same way. Experimentalists search for tiny EDM induced splitting of molecular magnetic sublevels in electric field. The goal of our work is to compute these tiny energy corrections for two candidate ions HBr^+ and HI^+. An additional goal is also to gain insights for other molecules T-odd energy corrections. The third goal of our work is to elucidate the influence of the nature of chemical bond on EDM splitting and ultimately, find how to make use of this it in order to choose more EDM-sensitive molecular ions.

I start this chapter by reviewing previous searches for the electron EDM with molecules and the newly proposed experiment with molecular ions. In section B, I present the model of molecular structure for the two ions of interest (HBr^+ and HI^+). In the same section I also describe computations of the electron EDM energy correction within this model. Section C introduces the notion of chemical bond in polar molecules. Section D and E treat respectively the ionic bond case (HBr^+)and the covalent bond case (HI^+). We found that the energy corrections due to EDM for the two ions differ by an unexpectedly large factor of fifteen because of the difference in the nature of the bond. Thus,we conclude, in section F, that because of this difference, one ion (HI^+) may be a potentially competitive candidate for the EDM search while the other ion (HBr^+) is not. Here again, atomic units are used throughout the chapter (see Appendix C for details on atomic units).

A. Introduction

The most stringent limits on electron EDM come from a table-top experiment with atomic Tl [13]. As with atoms, the internal energy states of heavy polar molecules can show

evidence of EDMs of the constituents. Compared to atomic experiments, where application of strong external E-field is required to enhance sensitivity, the experiments with polar molecules rather rely on the inner electric molecular field $\mathcal{E}_{\rm int}$ exerted upon the heavier atom. This field can be several orders of magnitude larger than the attainable laboratory fields. This notion, first elucidated by P.G.H.Sandars [28], has been exploited in experiments with YbF [29] and TlF [30–32] molecules. I also mention ongoing experiment with metastable PbO molecule[33].

A relatively small laboratory field is still required in the EDM experiments to polarize the molecule. Since the E-field would accelerate a charged particle out of an apparatus, EDM experiments are typically carried out using neutrals. It has been recently realized by Stutz and Cornell [18] that this limitation may be overcome with ion traps: electrostatic force exerted upon the ion by the polarizing E-field can average to zero if the polarizing field rotates rapidly in space, with the requisite spectroscopy then being performed in a rotating frame of reference. Moreover, the long coherence times in the trap would improve statistics compared to traditional beam and gas cell approaches. Because of this improved statistics, molecular ions with a relatively weak sensitivity to electron EDM could provide competitive constrains. In particular, the hydrogen halide ions HBr^+ and HI^+ in their lowest rovibrational state of the ground $X\,^2\Pi_{3/2}$ term are considered as attractive candidates for the proposed experiment [18].

As I mentioned above the goal of this work was two-fold. Firstly, we provided a guidance to emerging EDM searches with molecular ions [18] by computing EDM-induced energy corrections. Secondly, we elucidated the important role of the chemical bond in enhancement of electron EDM in molecular systems. While both HBr^+ and HI^+ ions have a similar electronic structure, the chemical bond in HBr^+ is of ionic nature, while for heavier HI^+ it is predominantly covalent[34, 35]. We found that this evolution in the character of the chemical bond has a marked effect on the EDM-induced energy corrections. From the experimental point of view, our computed EDM-induced energy correction for HBr^+ is too small to produce competitive bonds on the electron EDM in experiment [18]. By contrast, the pronounced covalent bond enhancement for the HI^+ ion, illuminated here, makes it a

potentially competitive candidate for the electron EDM search.

B. Molecular structure and EDM-induced corrections

The molecular structure of low-lying rotational states of hydrogen halide ions HBr^+ and HI^+ can be well classified by the Hund's case (a). Relativistic effects split the ground $X\,^2\Pi$ electronic term into two components: $^2\Pi_{3/2}$ and $^2\Pi_{1/2}$, distinguished by Ω, projection of the total electronic angular momentum along the molecular axis. $^2\Pi_{3/2}$ is the ground electronic term and it is considered as a possible candidate for the EDM experiment. In the estimates below we will employ the following values of the equilibrium internuclear separations [34, 35]: $R_e \approx 1.448$ $\mathring{A}$ for HBr^+ and $R_e \approx 1.632$ $\mathring{A}$ for HI^+. Unless noted otherwise, atomic units (Appendix C) are used throughout the paper.

In Hund's case (a) the molecular eigenfunctions including the nuclear rotation can be described as $|\Lambda\Sigma\Omega; JM_J\rangle = |JM_J\Omega\rangle\,|\Lambda\,\Sigma\,\Omega\rangle$, where Λ and Σ are projections of the electronic orbital momentum and spin onto the internuclear axis, J is the total molecular momentum (including nuclear rotation) and M_J is the laboratory frame projection of J. The rotational part $|JM_J\Omega\rangle$ may be expressed in terms of the Wigner D functions. While in the lowest-order $|\Lambda\Sigma\Omega; JM_J\rangle$ and $|-\Lambda-\Sigma-\Omega; JM_J\rangle$ states have the same energies, at the finer level each rotational state of the $^2\Pi_\Omega$ terms splits into so-called Λ–doublet [36] due to rotational and spin-orbit perturbations. The eigenstates of the field-free molecular Hamiltonian (disregarding EDM) are e/f parity states, composed of linear combinations of the two above states.

An externally applied electric field $\mathcal{E}_0$ couples the e/f parity states. For a sufficiently strong E-field the eigenstates can be classified by a definite value of Ω, rather than by the e/f parity label. In this case the correction to the energy due to electron EDM can be parameterized as [37] $\delta W(J, M, \Omega) = W_d\Omega$. It is defined as an expectation value

$$W_d\Omega = \langle\Lambda\Sigma\Omega; JM_J|\, H_e\,|\Lambda\Sigma\Omega; JM_J\rangle = \langle\Lambda\,\Sigma\,\Omega|H_e|\Lambda\,\Sigma\,\Omega\rangle\,. \tag{24}$$

Here,

$$H_e = 2d_e \begin{pmatrix} 0 & 0 \\ 0 & \sigma \cdot \mathcal{E} \end{pmatrix}, \tag{25}$$

is the pseudo-scalar coupling [12] of an electron EDM d_e to an electric field $\mathcal{E}$ (Appendix D). This internal molecular field is to be distinguished from the externally applied field. The expectation value (24) is accumulated in the region of strong fields, i.e., mainly in the vicinity of the nucleus of the heavier halogen atom. A common approximation is that the electric field is produced by a spherically symmetric charge distribution $\mathcal{E}(\mathbf{r}) \approx Z/r^2\,\hat{\mathbf{r}}$, where Z is the nuclear charge of the heavier atom, and $\mathbf{r} = 0$ coincides with its center.

C. Chemical bond

In the following we make an order-of-magnitude estimate of the EDM factor W_d using a qualitative model of an isolated atomic particle perturbed by its molecular counterpart. In this regard it is important to discuss the nature of the chemical bond in the hydrogen halide HX^+ ions. It can be be described by two limiting cases [35]: ionic (H^+:X) and covalent (H $\cdot\cdot$ X^+) bonds. In the case of the ionic bond the halogen atom is electrostatically perturbed by a proton. When the bond is covalent, the halogen atom is singly ionized (^3P state), while the hydrogen atom is in its ground state.

Although both HBr^+ and HI^+ ions dissociate to the covalent limit, the chemical bond at intermediate separations can be better characterized from molecular spectra. In particular, the hyperfine structure is of significance to our consideration, because both the EDM coupling and the hyperfine interaction are sensitive to behavior of the molecular orbitals near the nuclei. An analysis of the hyperfine structure in Ref. [34] indicates that the bond for the HBr^+ ion can be adequately described as being of the ionic nature. As to the HI^+ ion, the hyperfine-structure analysis by the same authors [35] shows that the bond is predominantly of the covalent character.

Below we consider both ionic and covalent bonds. Our semi-qualitative calculations follow a general scheme similar to those described in Ref. [12, 38]. Firstly, we determine the effective molecular electric field $\mathcal{E}_{\rm int}$ exerted upon the heavier halogen atom/ion. Then

we use the first-order perturbation theory in the interaction with $\mathcal{E}_{\rm int}$ to determine mixing of the atomic states of opposite parity. Finally we compute the expectation value of the EDM-coupling operator using *ab initio* relativistic atomic structure codes.

D. Ionic bond approximation for the HBr^+ ion

In the case of the ionic bond the halogen atom is electrostatically perturbed by a proton. In the spirit of the LCAO[1] method we expand the electronic wavefunction in terms of atomic states Φ_i of the halogen atom

$$|\Lambda\,\Sigma\,\Omega\rangle = \sum_i c_i |\Phi_i\rangle\,, \tag{26}$$

where the total angular momentum $J_{e,i}$ of the atomic state Φ_i and its projection on the molecular axis $M_{e,i}$ are constrained to $J_{e,i} \geq |\Omega|$ and $M_{e,i} = \Omega$. We determine the expansion coefficients c_i using the first order perturbation theory in the interaction V due to electrostatic field exerted upon the halogen atom by the proton

$$|\Lambda\,\Sigma\,\Omega\rangle \approx |\Phi_0\rangle + \sum_{i\neq 0} |\Phi_i\rangle \frac{\langle\Phi_i|V|\Phi_0\rangle}{E_0 - E_i}\,, \tag{27}$$

where Φ_0 is the ground atomic state of the proper symmetry and E_i are the energies of atomic states.

Keeping only the leading dipole term in the multipole expansion of the interaction of atomic electrons of the halogen atom with the proton, the perturbation $V \approx -\mathbf{D}\cdot\mathcal{E}_{\rm int}$, $\mathcal{E}_{\rm int}$ being the electric field of the proton at the position of the atom and $\mathbf{D}$ the atomic electric dipole operator. It is this strong electric field that produces enhancement of the electron EDM in molecular ions.

Finally, the EDM-induced energy correction is

$$W_d\Omega = \frac{2}{R_e^2} \sum_{i\neq 0} \frac{\langle\Phi_0|H_e|\Phi_i\rangle\langle\Phi_i|D_z|\Phi_0\rangle}{E_0 - E_i}\,. \tag{28}$$

In the following we will use a shorthand notation

$$T = H_e\,(E_0 - H_a)^{-1}\,D_z\,, \tag{29}$$

[1] Linear Combination of Atomic Orbitals

with H_a being the atomic Hamiltonian so that

$$W_d\Omega = \frac{2}{R_e^2}\,\langle\Phi_0|T|\Phi_0\rangle\,. \tag{30}$$

It is worth noting that all the quantities (except for empirical R_e) in the Eq. (28) are atomic ones and we employ atomic-structure methods to evaluate this sum. First we employ Dirac-Hartree-Fock (DHF) approximation and then more elaborate configuration-interaction (CI) method. All calculations carried out here are *ab initio* relativistic.

The halogen atoms Br and I are open-shell systems with one hole in the outer $np_{3/2}$-shell, $n = 4$ for bromine and $n = 5$ for iodine. In the DHF approximation the atomic orbitals $|i\rangle$ satisfy the eigenvalue equation $h_{\rm DHF}|i\rangle = \varepsilon_i|i\rangle$, where the Dirac Hamiltonian $h_{\rm DHF}$ includes an interaction with the field of the nucleus and the self-consistent field of the electrons. In the DHF approximation we obtain (see Appendix G for the derivation)

$$W_d\Omega = \frac{2}{R_e^2}\sum_i \frac{\langle g|h_e|i\rangle\langle i|d_z|g\rangle}{\varepsilon_i - \varepsilon_g}\,, \tag{31}$$

where g denotes the $np_{3/2}$ hole state and the summation over i extends over a complete set of orbitals, including both core and virtual orbitals. Before doing the numerical evaluation we can still reduce this expression (see Appendix H) to

$$W_d = \frac{4d_e}{R_e^2}\sum_i \frac{(-1)^{j_i-m_i}}{\varepsilon_i - \varepsilon_g}\begin{pmatrix} j_g & 1 & j_i \\ -m_g & 0 & m_i \end{pmatrix}\langle j_g||C^1||j_i\rangle\, R_D\, R_{EDM}\,, \tag{32}$$

where i denotes both core and virtual orbitals.

Numerically we carried out the summation using the B-spline pseudo-spectrum technique[27]. The pseudo-spectrum was generated using the DHF potential of the ground $^2P_{3/2}$ atomic state. In a typical calculation we used a set of basis functions expanded over 100 B-splines, which provided numerical accuracy sufficient for the goals of this paper. Among other technical details it is worth mentioning that while integrating the radial Dirac equation, we used the potential produced by a nucleus of the finite size.

To investigate a potentially large correlation effects beyond the DHF approximation, we have also carried out configuration-interaction (CI) calculations for Br within the active space of seven $4s^2\,4p^5$ valence electrons. In this method, the many-electron wave functions

were obtained as linear combinations of determinants composed from as single and double excitations of the valence electrons from the active space. Finally, following Dalgarno-Lewis-Steinheimer method [39], we carried out the summation over intermediate states in Eq. (37) by solving inhomogeneous many-body Dirac equation inherent to the method and computed the sum (28). More details will be provided elsewhere.

The resulting DHF value of the EDM-induced energy correction (hole in the $4p_{3/2}$ shell)

$$W_d\Omega[\mathrm{HBr}^+, \mathrm{ionic}, \mathrm{DHF}, \mathrm{X}\,^2\Pi_{3/2}] = -1.5 \times 10^{-2} d_e\,, \tag{33}$$

A similar DHF calculation assuming a hole in the $4p_{1/2}$ shell leads to a 100-fold increase in the value of the EDM correction

$$W_d\Omega[\mathrm{HBr}^+, \mathrm{ionic}, \mathrm{DHF}, \mathrm{X}\,^2\Pi_{1/2}] = 1.6 d_e\,. \tag{34}$$

A large difference in the values of the $W_d\Omega$ parameter for the two cases can be explained as follows. The EDM-coupling operator H_e is a pseudo-scalar: it does not change the total angular momentum of a state, but flips its parity. For example, if the hole state g has $p_{3/2}$ angular character, then the intermediate states in Eq.(31) are $d_{3/2}$ orbitals. Similarly, the $p_{1/2}$ hole state requires $s_{1/2}$ intermediate states. It is well known [12], that since the states of lower orbital momentum have a larger probability to be found close to the nucleus, this selection rule has a profound effect on the order of magnitude of the EDM factor W_d.

One may argue that an enhancement of the EDM factor for the $X\,^2\Pi_{3/2}$ state may arise due to particle-hole excitations, when $s_{1/2}$ ($p_{1/2}$) electron is excited from the core to the $p_{1/2}$ ($s_{1/2}$) orbital. It is easy to demonstrate in the DHF approximation, that while the individual contributions from such excitations are certainly large, their sum vanishes. It is the reason why the closed-shell systems are largely insensitive to the electron EDM [12], i.e the EDM-induced energy correction arises only due to an unpaired electron. Correlations (many-body effects beyond DHF) may potentially spoil the presented argument and we have carried out the correlated CI calculations. The result,

$$W_d\Omega[\mathrm{HBr}^+, \mathrm{ionic}, \mathrm{CI}, \mathrm{X}\,^2\Pi_{3/2}] = -2.6 \times 10^{-2} d_e\,, \tag{35}$$

is of the same order as the DHF value.

As a reference, here we also present the DHF value for the HI^+ ion in the ionic bond approximation

$$W_d\Omega[\mathrm{HI}^+, \mathrm{ionic}, \mathrm{DHF}, \mathrm{X}\,^2\Pi_{3/2}] = -7.0 \times 10^{-2} d_e\,. \tag{36}$$

E. Covalent bond approximation for HI^+

From the preceding discussion it is clear that a participation of the unpaired $p_{1/2}$ or $s_{1/2}$ orbital in the ground-state configuration of the heavier molecular constituent is important for gaining large W_d parameter. Qualitatively we can hope that such an enhancement for the $X^2\Pi_{3/2}$ component may arise when the chemical bond acquires covalent character (case of HI^+ ion). Indeed, in the covalent bond approximation, the halogen atom becomes singly ionized its ground state being ^3P. The ground state has two p holes in the outer shell, so that the corresponding relativistic many-body states are composed from linear combination of $p_{1/2}^{-1}\,p_{1/2}^{-1}$, $p_{3/2}^{-1}\,p_{1/2}^{-1}$ and $p_{3/2}^{-1}\,p_{3/2}^{-1}$ single- electron configurations (the superscript -1 designates a hole state). Therefore the unpaired $j = 1/2$ orbital becomes involved in the calculations, and indeed, as shown below, this leads to a significantly larger EDM-induced energy correction for the $X^2\Pi_{3/2}$ term.

The HI^+ ion may be pictured as the iodine ion I^+ in the ^3P state perturbed by the neutral hydrogen atom in its ground state. First let us derive the internal electric field $\mathcal{E}_{\rm int}$ and the associated mixing of opposite parity states of the iodine ion. Qualitatively, the field of I^+ induces a dipole moment of the hydrogen atom $|D_H| = \alpha_0/R_e^2$, where $\alpha_0 = 9/2$ is the polarizability of the hydrogen ground state. In turn, the induced dipole moment exerts a field at the position of the iodine ion $\mathcal{E}_{int} = 2\alpha_0/R_e^5\hat{z}$. Thus the iodine ion is perturbed by $V \approx -2\alpha_0 D_z/R_e^5$, where D is the atomic dipole moment operator for I^+.

Again we limit our consideration to a qualitative estimate and use the first-order perturbation theory in the molecular field, so that the EDM-induced energy correction is

$$W_d\Omega = -\frac{4\alpha_0}{R_e^5}\,\langle\Phi_0|T|\Phi_0\rangle\,, \tag{37}$$

where the operator T is given by Eq. (29), except now all the participating operators in that expression are to be understood as being for the iodine ion and Φ_0 is its properly

symmetrized ground state. The above expression differs from the analogous formula (30) for the ionic bond by a prefactor characterizing the internal molecular field $\mathcal{E}_{\rm int}$ acting upon the halogen atom/ion. Compared to the ionic bond, this perturbing field becomes 70% weaker.

In order to carry out the calculations with the relativistic operator H_e, we express the unperturbed non-relativistic molecular wavefunction in terms of the relativistic wave-functions of the iodine ion, $|^3P_J, M_{I^+}\rangle$, and the hydrogen, $\left|1s_{1/2}, M_{\rm H}\right\rangle$,

$$\left|^2\Pi_{3/2}\right\rangle^{(0)}_{\rm covalent} = \sqrt{\frac{2}{3}}\left|^3P_2, 2\right\rangle\left|1s_{1/2}, -\frac{1}{2}\right\rangle + \\ -\sqrt{\frac{1}{6}}\left(\left|^3P_2, 1\right\rangle\left|1s_{1/2}, \frac{1}{2}\right\rangle + \left|^3P_1, 1\right\rangle\left|1s_{1/2}, \frac{1}{2}\right\rangle\right) . \tag{38}$$

Since the expectation value of the EDM coupling operator H_e is accumulated close to the nucleus of the heavy iodine ion, H_e is essentially a one-center operator and a generalization of Eq.(37) for the two-center wavefunction (39) reads

$$\left(-\frac{4\alpha_0}{R_e^5}\right)^{-1}\langle^2\Pi_{3/2}|H_e|^2\Pi_{3/2}\rangle_{\rm covalent} = \\ \frac{3}{2}\left\langle^3P_2, 1\right|T\left|^3P_2, 1\right\rangle + \frac{1}{6}\left\langle^3P_1, 1\right|T\left|^3P_1, 1\right\rangle + \\ \frac{1}{6}\left\langle^3P_2, 1\right|T\left|^3P_1, 1\right\rangle + \frac{1}{6}\left\langle^3P_1, 1\right|T\left|^3P_2, 1\right\rangle , \tag{39}$$

We calculated the values of matrix elements for iodine ion within the CI approach similar to the one described above for Br. The computed values are $\langle^3P_2, 1|\,T\,|^3P_2, 1\rangle = 6.4\,d_e$, $\langle^3P_1, 1|\,T\,|^3P_1, 1\rangle = -13.4\,d_e$, $\langle^3P_1, 1|\,T\,|^3P_2, 1\rangle = -11.2\,d_e$, and $\langle^3P_2, 1|\,T\,|^3P_1, 1\rangle = 2.5\,d_e$. Finally,

$$W_d\Omega[{\rm HI}^+, {\rm covalent}, {\rm CI}, {\rm X}\,^2\Pi_{3/2}] = -0.4 d_e\,. \tag{40}$$

We notice a sizable enhancement compared to the value of $-7\times10^{-2}d_e$ obtained in the ionic bond approximation.

F. Conclusions

First of all the EDM-induced energy correction for the $X^2\Pi_{3/2}$ state of HI^+ is about 15 times larger than for HBr^+. A lesser part of this enhancement comes from the well-known

Z^3 scaling of CP-violating matrix elements [12], when bromine ($Z = 35$) is replaced by the heavier iodine ($Z = 53$). A more substantial factor, illuminated in this work, is the evolution in the nature of the chemical bond. To reiterate, the CP-violating matrix elements are much larger for the $p_{1/2}$ states than for $p_{3/2}$, due to the fact that the values of the relevant matrix elements are accumulated close to the nucleus. In the ionic bond case of HBr^+, the EDM correction arises from an unpaired $p_{3/2}$ hole state in the outer shell and CP-violating effects are suppressed. By contrast, the covalent bond of HI^+ in addition opens the $p_{1/2}$ shell, leading to a marked enhancement.

Typical values [37, 40] of the EDM-induced energy corrections for heavy *neutral* polar molecules PbO and YbF are on the order of $10d_e$ atomic units. Our computed value for HI^+ is an order of magnitude smaller. Yet, when compared with the conventional beam and gas-cell experiments, the proposed trapping experiment [18] has a better statistical sensitivity so that molecular ions with smaller enhancement parameters, such as HI^+, may suffice. By contrast, the EDM correction for HBr^+ is too small to be of experimental interest. As shown here, it is the covalent bond of HI^+ that makes this ion a potentially competitive candidate for the emerging searches for EDMs with molecular ions.

IV. T-ODD POLARIZABILITY OF Xe ATOM IN LIQUID Xe

T-violating effects lead to a tiny magnetization of a sample placed in an electric field. They also lead to a tiny electrical polarization of a sample placed in a magnetic field. Current techniques allow experimentalists to measure very small magnetic fields. In this chapter, I look at the possibility, with available techniques, of measuring a tiny T-violating magnetic field coming from a material placed in a huge electric field. As we have discussed in Chapter II, liquid Xe could be a good material to use for this experiment due to its properties. While the T-violation considered in chapter II was due to nuclear sources, here it would mainly come from the electron EDM as in Chapter III. As a consequence, measuring a T-violating magnetic field could set a limit on the electron EDM.

In this chapter, the T-odd polarizability is estimated for the rare-gas atoms He through Rn. The results show that the T-odd polarizability of rare-gas atoms scales as $Z^5R(Z)$, where Z is the nuclear charge and $R(Z)$ is a slowly varying relativistic enhancement factor. It is found that liquid Xe experiment could provide competitive bounds on the electron EDM only if the present level of experimental sensitivity to ultraweak magnetic fields [41] is improved by several orders of magnitude.

The chapter is organized as follows: In section B, I derive the third-order expression for the T-violating polarizability $\beta^{\rm CP}$ and use the independent-particle approximation to simplify the atomic many-body expressions. In section C, I present results of Dirac-Hartree-Fock (DHF) calculations of $\beta^{\rm CP}$ for rare-gas atoms and derive the Z scaling of $\beta^{\rm CP}$. In section D, I evaluate a feasibility of setting a limit on electron EDM by measuring T-violating magnetization of liquid Xe. Finally, in section E the conclusions are drawn.

A. Introduction

Interaction of an atom with external DC electric field $\mathcal{E}_0$ in the presence of the electron EDM causes spin polarization in the direction of the field [42]. As a consequence, a magnetic moment $\mu^{\rm CP}$ is induced by an electric field, $\mu^{\rm CP} = \beta^{\rm CP}\mathcal{E}_0$. The first attempt to measure corresponding magnetization of the ferromagnetic crystal was made by Vasiliev and

Kolycheva in 1978 [43]. According to Lamoreaux [44], modern techniques allow to improve that old measurement by many orders of magnitude and reach the sensitivity, which allows to improve the present limit on the electron EDM ($d_e(\mathrm{Tl}) < 1.6 \times 10^{-27} e\,\mathrm{cm}$). Results of the new generation of experiments with ferromagnetic solids were recently reported by Hunter [45]. A characteristic feature of the experiments with macroscopic magnetization is the dependence of the signal on the density of atoms. That gives a huge enhancement in sensitivity for a condensed phase sample.

It is generally assumed that diamagnetic atoms are not useful for the search of the electron EDM. However, Baryshevsky has recently pointed out [46] that T-violating magnetization would also exist for a diamagnetic atom. For a spherically symmetric atom, the E-field-induced magnetic moment μ^{CP} can be expressed in terms of T-violating polarizability β^{CP} as

$$\mu^{\mathrm{CP}} = \beta^{\mathrm{CP}} \mathcal{E}_0, \tag{41}$$

where $\mathcal{E}_0$ is the strength of the electric field. This observation opens interesting experimental possibilities. For example, one can measure magnetization of liquid xenon in a strong external electric field. The advantage of the experiment with diamagnetic liquid in comparison to ferromagnetic solids is a much lower magnetic noise. For a diamagnetic (closed-shell) atom the magnetization (41) appears in the higher orders of the perturbation theory than for the open-shell atoms.

We find that the T-violating polarizability exhibits an unusually strong dependence on the nuclear charge Z. Previously, Sandars [47] has shown that an atomic enhancement factor for the electron EDM is of the order of $\alpha^2 Z^3$, where $\alpha = 1/137$ is the fine-structure constant. As we demonstrate in section C, for a diamagnetic atom, the polarizability β^{CP} vanishes in the nonrelativistic approximation. Because of that it is suppressed by a factor of $(\alpha Z)^2$. With the Sandars enhancement factor this leads to a steep, Z^5, scaling of the effect.

Finally, we evaluate the feasibility of setting a limit on electron EDM by measuring T-violating magnetization of liquid Xe. To consider the effect of the environment on β^{CP} in the liquid state, we use the exact same techniques described in Chapter II: we solve the DHF equation in a spherically symmetric cavity with proper boundary conditions. We

find that compared to the T-odd polarizability of an isolated Xe atom, the resulting T-odd polarizability of an atom of liquid Xe is suppressed by about 65%.

B. Formalism

In this section we derive the expression for T-violating polarizability within the third-order perturbation theory. Further, we simplify the derived expression using the Dirac-Hartree-Fock approximation for atomic many-body states.

The problem to be solved can be formulated as follows: What is the induced magnetic moment $\langle \boldsymbol{\mu} \rangle$ of an atom perturbed by an external electric field $\mathcal{E}_0$? As I explained in section IB2, if the atomic wavefunctions are the eigenstates of the parity and time-reversal operators, the induced magnetic moment vanishes. However, in the presence of the T-odd interactions, $V^{\rm CP}$, there appears a tiny E-field-induced magnetic moment. To emphasize the essential role of T or CP-violation in the generation of the magnetic-moment, we will use CP superscript with the magnetic moment, $\left\langle \boldsymbol{\mu}^{\rm CP} \right\rangle$ (T is equivalent to CP according to the CPT theorem, see section IA3). The interaction $V^{\rm CP}$ is due to the electron EDM. For a spherically-symmetric system, the induced magnetic moment will be directed along the applied E-field.

Remark: CP-odd weak neutral-current interactions between electrons and the nucleus also contribute to an atomic magnetic moment. This contribution is indistinguishable from the electron EDM. We will have to specify the particular forms of $V^{\rm CP}$ for each contributions.

1. *Third-order formula for the induced magnetic moment*

We develop the perturbative expansion for the atomic wavefunction $|\Psi_0\rangle$ in terms of the combined interaction $W = V^{\rm CP} + V^{\rm ext}$. Here $V^{\rm ext}$ is the interaction with the external electric field applied along the z-axis, $V^{\rm ext} = -D_z\,\mathcal{E}_0$, D_z being the z-component of the electric dipole moment operator. To estimate the dominant contribution to $\langle \boldsymbol{\mu} \rangle$, it is sufficient to truncate the perturbative expansion for the atomic wavefunction at the second order in W,

$|\Psi_0\rangle \approx |\Psi_0^{(0)}\rangle + |\Psi_0^{(1)}\rangle + |\Psi_0^{(2)}\rangle$. Then the expectation value of the magnetic moment reads

$$\left\langle \boldsymbol{\mu}^{\rm CP} \right\rangle = \langle \Psi_0^{(1)} | \boldsymbol{\mu} | \Psi_0^{(1)} \rangle + \langle \Psi_0^{(0)} | \boldsymbol{\mu} | \Psi_0^{(2)} \rangle + \langle \Psi_0^{(2)} | \boldsymbol{\mu} | \Psi_0^{(0)} \rangle \,. \tag{42}$$

To arrive at the above expression we used a simplifying fact that the magnetic moment is a P-even operator, while both $|\Psi_0^{(0)}\rangle$ and $|\Psi_0^{(2)}\rangle$ have parities opposite to the one of the first-order correction $|\Psi_0^{(1)}\rangle$.

The textbook expressions for the first and second-order corrections to wavefunctions can be found, for example, in Ref. [48]. With these expressions,

$$\left\langle \boldsymbol{\mu}^{\rm CP} \right\rangle = \left\langle \boldsymbol{\mu}^{\rm CP} \right\rangle_1 + \left\langle \boldsymbol{\mu}^{\rm CP} \right\rangle_2 + \left\langle \boldsymbol{\mu}^{\rm CP} \right\rangle_3 , \tag{43}$$

$$\left\langle \boldsymbol{\mu}^{\rm CP} \right\rangle_1 = 2 \sum_{kl} \frac{V_{0k}^{\rm CP}}{E_0 - E_k} \boldsymbol{\mu}_{kl} \frac{V_{l0}^{\rm ext}}{E_0 - E_l} \,, \tag{44}$$

$$\left\langle \boldsymbol{\mu}^{\rm CP} \right\rangle_2 = 2 \sum_{kl} \boldsymbol{\mu}_{0k} \frac{V_{kl}^{\rm CP}\, V_{l0}^{\rm ext}}{(E_0 - E_k)\,(E_0 - E_l)} \,, \tag{45}$$

$$\left\langle \boldsymbol{\mu}^{\rm CP} \right\rangle_3 = 2 \sum_{kl} \boldsymbol{\mu}_{0k} \frac{V_{kl}^{\rm ext}\, V_{l0}^{\rm CP}}{(E_0 - E_k)\,(E_0 - E_l)} \,. \tag{46}$$

In these formulas, the summations are carried out over the eigenstates of the atomic Hamiltonian H_a, $H_a|\Psi_p^{(0)}\rangle = E_p|\Psi_p^{(0)}\rangle$. The derived third-order expression can be presented in a more compact and symmetrical form using the resolvent operator $\mathcal{R} = (E_0 - H_a)^{-1}$,

$$\begin{aligned} \left\langle \boldsymbol{\mu}^{\rm CP} \right\rangle = \;& 2\langle 0 | V^{\rm CP}\, \mathcal{R}\, \boldsymbol{\mu}\, \mathcal{R}\, V^{\rm ext} | 0 \rangle \\ + \;& 2\langle 0 | \boldsymbol{\mu}\, \mathcal{R}\, V^{\rm CP} \mathcal{R}\, V^{\rm ext} | 0 \rangle \\ + \;& 2\langle 0 | \boldsymbol{\mu}\, \mathcal{R}\, V^{\rm ext}\, \mathcal{R}\, V^{\rm CP} | 0 \rangle \,. \end{aligned} \tag{47}$$

The three above contributions differ by permutations of the operators $\boldsymbol{\mu}$, $V^{\rm CP}$ and $V^{\rm ext}$.

2. Dirac-Hartree-Fock approximation

Having derived a general third-order expression for the induced magnetic moment, Eq. (48), here we proceed with the atomic-structure part of the evaluation. We employ the conventional Dirac-Hartree-Fock (DHF) or independent-particle approximation for that purpose. In this approach, the atomic many-body wavefunction is represented by the Slater determinant composed of single-particle orbitals. These orbitals are determined from a set

of the DHF equations. Using a complete set of Slater determinants, the contributions to the induced magnetic moment, Eq.(44–46), may be expressed as

$$\left\langle \boldsymbol{\mu}^{\rm CP} \right\rangle_{1,a} = 2 \sum_{amn} \frac{V^{\rm CP}_{an} \boldsymbol{\mu}_{nm} V^{\rm ext}_{ma}}{(\varepsilon_m - \varepsilon_a)(\varepsilon_n - \varepsilon_a)} \,, \tag{48}$$

$$\left\langle \boldsymbol{\mu}^{\rm CP} \right\rangle_{1,b} = -2 \sum_{abm} \frac{V^{\rm CP}_{bm} \, \boldsymbol{\mu}_{ab} \, V^{\rm ext}_{ma}}{(\varepsilon_m - \varepsilon_a)\,(\varepsilon_m - \varepsilon_b)}, \tag{49}$$

$$\left\langle \boldsymbol{\mu}^{\rm CP} \right\rangle_{2,a} = 2 \sum_{amn} \frac{\boldsymbol{\mu}_{an} V^{\rm CP}_{nm} \, V^{\rm ext}_{ma}}{(\varepsilon_m - \varepsilon_a)\,(\varepsilon_n - \varepsilon_a)} \,, \tag{50}$$

$$\left\langle \boldsymbol{\mu}^{\rm CP} \right\rangle_{2,b} = -2 \sum_{abm} \frac{\boldsymbol{\mu}_{bm} V^{\rm CP}_{ab} \, V^{\rm ext}_{ma}}{(\varepsilon_m - \varepsilon_a)\,(\varepsilon_m - \varepsilon_b)}, \tag{51}$$

$$\left\langle \boldsymbol{\mu}^{\rm CP} \right\rangle_{3,a} = 2 \sum_{amn} \frac{\boldsymbol{\mu}_{an} V^{\rm ext}_{nm} \, V^{\rm CP}_{ma}}{(\varepsilon_m - \varepsilon_a)\,(\varepsilon_n - \varepsilon_a)} \,, \tag{52}$$

$$\left\langle \boldsymbol{\mu}^{\rm CP} \right\rangle_{3,b} = -2 \sum_{abm} \frac{\boldsymbol{\mu}_{bm} V^{\rm ext}_{ab} \, V^{\rm CP}_{ma}}{(\varepsilon_m - \varepsilon_a)\,(\varepsilon_m - \varepsilon_b)} \,. \tag{53}$$

Here indexes a and b run over single-particle orbitals occupied in $|\Psi_0\rangle$, indexes m and n run over virtual orbitals, and ε_i are the energies of the HF orbitals.

It is well known that the relativistic effects are essential for the non-vanishing contributions to energy levels due to EDMs. Moreover, in section IV C 1, we will demonstrate that relativity enters into the calculations of T-violating polarizability in the enhanced fashion: one also needs to incorporate relativistic corrections to electric- and magnetic-dipole matrix elements and energies entering Eq.(44–46). We include the relativistic effects by directly solving Dirac-Hartree-Fock (DHF) equations

$$\left(c(\boldsymbol{\alpha} \cdot \boldsymbol{p}) + \beta c^2 + V_{\rm nuc} + V_{\rm DHF}\right) u_i(\boldsymbol{r}) = \varepsilon_i u_i(\boldsymbol{r}) \,, \tag{54}$$

where $V_{\rm nuc}$ is a potential of the Coulomb interaction with a finite-size nucleus and $V_{\rm DHF}$ is non-local self-consistent DHF potential.

At this point we would like to specify particular forms for the T or CP-odd interaction $V^{\rm CP}$. We will distinguish between the electron EDM coupling $V^{\rm CP,EDM}$ and weak neutral-current (NC) interactions $V^{\rm CP,NC}$. The formula for both contributions can be found in Appendix D. The matrix elements between single-particle orbitales are shown in Appendix E. We can now treat the numerical part which will give us the results in the next section.

C. Results for rare-gas atoms

The derived DHF expressions hold for any atomic or molecular system with a state composed from a single Slater determinant. Below we carry out calculations for the rare-gas atoms He through Rn. These closed-shell atoms have a $^1S_0$ ground state and, due to the spherical symmetry, the CP-violating polarizability is a scalar quantity, i.e., the induced magnetic moment is parallel to the applied electric field. The intermediate many-body states in Eq. (44–46) are particle-hole excitations, with the total angular momenta of $J = 0$ or $J = 1$, depending on the multipolarity of the involved operator.

As in chapter II, we solve the DHF equations in the cavity using a B-spline basis set technique by W.R.Johnson and J.Sapirstein [27]. The resulting set of basis functions is finite and can be considered as numerically complete. In a typical calculation we used a set of basis functions expanded over 100 B-splines. An additional peculiarity related to the Dirac equation is an appearance of negative energy states ($\varepsilon_m < -m_e c^2$) in the summation over intermediate states in Eq. (48)–(53). In our calculations we used the so-called length-form of the electric-dipole operator, Eq. (E2) and we found the contribution of negative-energy-state to be insignificant.

Atom	Z	$\beta^{\rm CP}/d_e$	$\beta^{\rm CP}/K$
He	2	$-3.8[-9]$	$-2.4[-22]$
Ne	10	$-2.2[-6]$	$-1.5[-19]$
Ar	18	$-7.4[-5]$	$-5.2[-18]$
Kr	36	$-3.6[-3]$	$-3.1[-16]$
Xe	54	$-4.5[-2]$	$-5.3[-15]$
Rn	86	-1.07	$-2.2[-13]$

TABLE IV: CP-violating polarizability, $\beta^{\rm CP}$, in Gaussian atomic units, for rare-gas atoms. CP-violation is either due to the electron EDM, d_e, or due to the neutral currents (D5). Notation $x[y]$ stands for $x \times 10^y$.

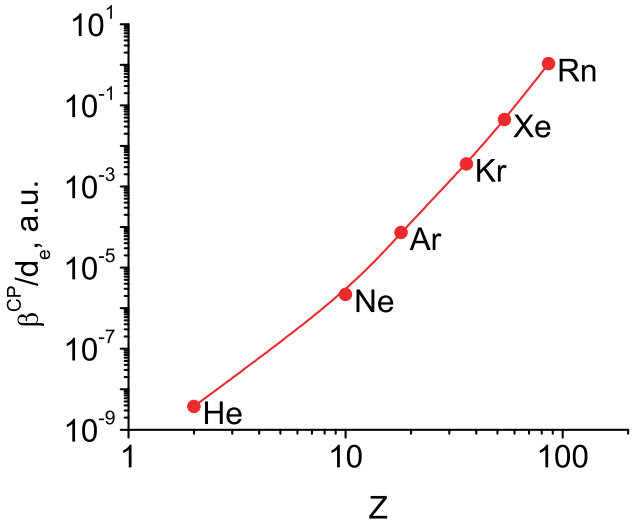

FIG. 7: Dependence of the T-violating polarizability $\beta^{\rm CP}$ on the nuclear charge Z for rare-gas atoms. T-violation is due to the electron EDM, d_e. The ratio $\beta^{\rm CP}/d_e$ is given in atomic units.

Numerical results for rare-gas atoms are presented in Table IV and also plotted in Fig. 7. In Table IV, the values in the column marked $\beta^{\rm CP}/d_e$ were computed directly, while the values $\beta^{\rm CP}/K$ (the last column) were obtained from $\beta^{\rm CP}/d_e$ as explained in section IV C 1.

From Fig. 7 we observe a pronounced dependence of the values on the nuclear charge Z. Such a steep scaling of the T-odd polarizabilities is expected from the considerations presented in section IV C 1.

To illustrate the (doubly) relativistic origin of the T-odd polarizability $\beta^{\rm CP}$, we compile values of various contributions to $\beta^{\rm CP}$ in Table V for an isolated Xe atom. Apparently, the dominant contributions are from $\langle\mu^{\rm CP}\rangle_{1,a}$, Eq. (48), and $\langle\mu^{\rm CP}\rangle_{1,b}$, Eq. (49), but there is strong cancelation between these two terms. As we will see below, this cancelation is not accidental.

1. *Z^5 scaling and relation between EDM and NC contributions*

Let us consider non-relativistic limit of Eqs. (44 – 46). The magnetic moment operator is reduced to the form:

$$\boldsymbol{\mu} = -\frac{\alpha}{2}(2\boldsymbol{s} + \boldsymbol{l}). \tag{55}$$

k	$\beta^{\rm CP}_{k,a}/d_e$	$\beta^{\rm CP}_{k,b}/d_e$	sum
1	0.108	−0.132	−2.44[−2]
2	−6.53[−3]	6.63[−5]	−6.46[−3]
3	−8.19[−3]	−5.13[−3]	−1.33[−2]
total			−4.42[−2]

TABLE V: Contributions to T-violating polarizability, $\beta^{\rm CP}/d_e$, in Gaussian atomic units, for an isolated Xe atom. Each contribution is defined via Eq. (48)–(53) as $\beta^{\rm CP}_{k,\alpha}/d_e = \langle\mu^{\rm CP}\rangle_{k,\alpha}/(d_e\mathcal{E}_0)$. CP-violation is due to the electron EDM, d_e. Notation $x[y]$ stands for $x\times 10^y$.

This operator can not change electronic principal quantum numbers. Because of that the contributions (45) and (46) vanish, as there $\boldsymbol{\mu}$ should mix occupied and excited orbitals. Thus, we are left with the single term (44), which can be further split in two parts (48) and (49). We will show now that these two parts cancel each other.

Indeed, in the non-relativistic approximation the operator $V^{\rm CP}$ is given by a scalar product of the spin vector and the orbital vector. Therefore, in the LS-coupling scheme it can couple the ground state $^1S_0$ only to the excited states $^3P_0$. Operator (55) is diagonal in the quantum numbers L and S and can couple $^3P_0$ only to $^3P_1$. To return back to the ground state, the dipole operator $V^{\rm ext}$ has to couple $^3P_1$ to $^1S_0$. However, this matrix element vanishes in the non-relativistic approximation. The above states $^3P_{0,1}$ are formed from the excited electron and a whole in the core, which correspond to two expressions (48) and (49). We conclude that these two contributions exactly cancel in the non-relativistic approximation.

The matrix element $\langle{}^3P_1|V^{\rm ext}|{}^1S_0\rangle$ is proportional to the spin-orbit mixing, which is of the order of $(\alpha Z)^2$. It follows from (E1) that relativistic correction to operator (55) is of the same order. This correction accounts for the nondiagonal in the principle quantum numbers matrix elements of $\boldsymbol{\mu}$ and leads to the nonzero values of the terms (45) and (46). Thus, we see that all three terms in (43) are suppressed by the relativistic factor $(\alpha Z)^2$, in agreement with numerical results from Table V.

Matrix elements of the T-odd interaction $V^{\rm CP}$ depend on the short distances and rapidly

decrease with quantum number j. To a good approximation it is possible to neglect all matrix elements for $j \geq 3/2$. For the remaining matrix elements between orbitals $s_{1/2}$ and $p_{1/2}$ an analytical expression can be found in [49]:

$$\langle s_{1/2}|V^{\rm CP,EDM}|p_{1/2}\rangle = \frac{16}{3}\frac{\alpha^2 Z^3 R^{\rm EDM}}{(\nu_s\nu_p)^{3/2}}d_e, \tag{56}$$

$$\langle s_{1/2}|V^{\rm CP,NC}|p_{1/2}\rangle = \frac{G_{\rm F}}{2\sqrt{2}\pi}\frac{\alpha Z^3 R^{\rm NC}}{(\nu_s\nu_p)^{3/2}}K, \tag{57}$$

where we use effective quantum numbers $\nu = (-2\varepsilon)^{-1/2}$. $R^{\rm EDM}$ and $R^{\rm NC}$ are relativistic enhancement factors:

$$R^{\rm EDM} = \frac{3}{\gamma(4\gamma^2-1)} = \begin{cases} 1, & Z = 1, \\ 1.4, & Z = 54, \ \text{(Xe)}, \\ 2.7, & Z = 86, \ \text{(Rn)}, \end{cases} \tag{58}$$

$$R^{\rm NC} = \frac{4\gamma(2Zr_{\rm N})^{2\gamma-2}}{\Gamma^2(2\gamma+1)} = \begin{cases} 1, & Z = 1, \\ 2.5, & Z = 54, \\ 8.7, & Z = 86, \end{cases} \tag{59}$$

where Γ is the Gamma function, $\gamma = \sqrt{1-(\alpha Z)^2}$ and the radius of the nucleus is taken to be $r_{\rm N} = 1.2\,(Z+N)^{1/3}$fm [49].

We see that both T-odd operators scale as Z^3R with relativistic enhancement factors R given by (58) and (59). This scaling adds up with relativistic suppression $(\alpha Z)^2$ discussed above to give overall scaling Z^5R. This scaling agrees with our numerical calculations and Fig. 7.

Because of the similarity between matrix elements (56) and (57) of operators $V^{\rm CP,EDM}$ and $V^{\rm CP,NC}$, there is no need in calculating independently the NC contribution to $\beta^{\rm CP}$. It is sufficient to substitute matrix elements (56) in all equations with matrix elements (57). Comparing these expressions we find that to get the contribution to $\beta^{\rm CP}$ induced by the CP-odd weak neutral currents we need to make following substitution:

$$\frac{d_e}{er_0} \Longleftrightarrow 0.64\times 10^{-13}\frac{R^{\rm NC}}{R^{\rm EDM}}K, \tag{60}$$

where r_0 is the Bohr radius and $R^{\rm EDM}$ and $R^{\rm NC}$ are given by (58) and (59). The accuracy of (60) is typically 15 – 20%, which is sufficient for our purposes. It was used to calculate the last column of Table IV.

D. Limits on electron EDM from measurement of T-odd polarizability

Here we envision the following experimental setup (see Fig. 8) to measure the T-violating polarizability: A strong electric field $\mathcal{E}_0$ is applied to a sample of diamagnetic atoms of number density n. A macroscopic magnetization arises due to the T-violating polarizability. This magnetization generates a very weak magnetic field B. One could measure this induced magnetic field and set the limits on the electron EDM or other T-violating mechanisms. In particular, for a spherical cell the maximum value of the generated magnetic field at the surface of the sphere can be related to the T-violating polarizability as

$$B_{\rm max} = \frac{8\pi}{3} n\, \beta^{\rm CP} \mathcal{E}_0\,. \tag{61}$$

Clearly, one should increase the number density to enhance the signal, and it is beneficial to work with a dense liquid or solid sample.

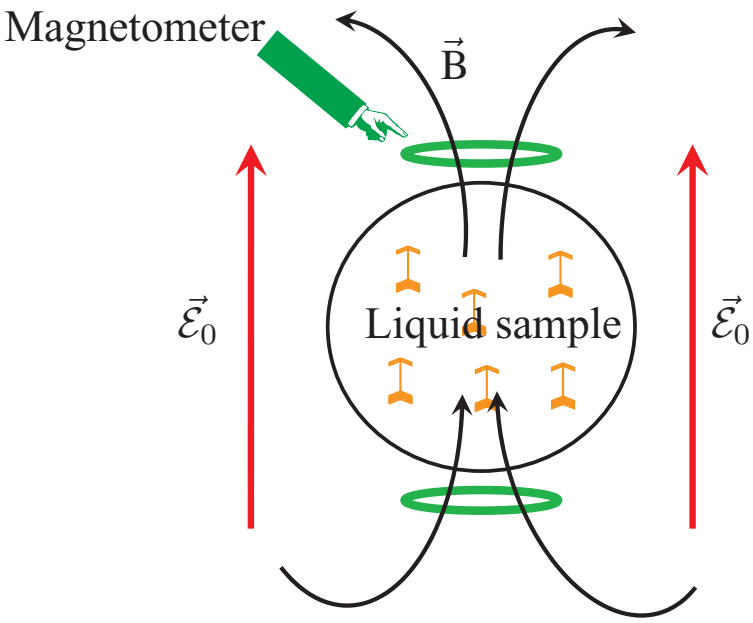

FIG. 8: (Color online) A scheme for measuring T-violating polarizability.

Among the rare-gas atoms, considered here, xenon has the most suitable properties for such an experiment: Xe is the heaviest non-radioactive atom, it has a large number density ($n \sim 10^{22}\,1/\text{cm}^3$), and liquid Xe has a high electric field breakdown strength ($\mathcal{E}_0 \sim 4 \times 10^5 \text{V/cm}$). Our calculations in section IV C were carried out for isolated atoms. However, in a liquid, there are certain environmental effects (such as confinement of electronic density)

that affect the T-violating signal. To estimate the confinement effects in the liquid, we employ the liquid-cell model. The calculations are similar to those of Chapter II. In brief, we solve the DHF equations for a Xe atom in a spherical cavity of radius $R_{\rm cav} = \left(\frac{3}{4\pi}\,\frac{1}{n}\right)^{1/3}$, with certain boundary conditions imposed at the cavity surface. For a density of liquid Xe of 500 amagat [50], $R_{\rm cav} \simeq 4.9$ bohr. For a solid state, $R_{\rm cav} \simeq 4.2$ bohr and we use the latter in the calculations for the same reasons as in Chapter II. Technically, we applied the variational Galerkin method on a set of 100 B-spline functions [27]. We find numerically that compared to an isolated atom, the T-violating polarizability of a Xe atom in liquid Xe is reduced by about 65%,

$$\beta^{\rm CP}({\rm LXe}) \approx 1.5 \times 10^{-2} d_e\,. \tag{62}$$

From Eq. (61) it is clear that the more sensitive the measurement of the B-field, the tighter the constraints on $\beta^{\rm CP}$ (and d_e) are. Presently, the most sensitive measurement of weak magnetic fields has been carried out by Princeton group [51]. Using atomic magnetometry, this group has reached the sensitivity level of $5.4 \times 10^{-12}\,{\rm G}/\sqrt{\rm Hz}$. The projected theoretical limit [51] of this method is $10^{-13}\,{\rm G}/\sqrt{\rm Hz}$. Notice that this estimate has been carried out for a sample of volume 0.3 cm^3. According to Romalis [52], the sensitivity increases with volume V as $V^{1/3}$, so a 100 cm^3 cell would have an even better sensitivity of about $10^{-14}\,{\rm G/Hz}^{1/2}$. More optimistic estimate, based on nonlinear Faraday effect in atomic vapors [53], is given in Ref.[44]; here the projected sensitivity is $3 \times 10^{-15}\,{\rm G}/\sqrt{\rm Hz}$.

Assuming 10 days of averaging, the most optimistic published estimate of the sensitivity to magnetic field [44] leads to the weakest measurable field of $B \simeq 3 \times 10^{-18}\,{\rm G}$. Combining this estimate with the breakdown strength of the E-field for liquid Xe, $\mathcal{E}_0 \sim 4 \times 10^5\,{\rm V/cm}$, and our computed value of T-odd polarizability, Eq. (62), we arrive at the constraint on the electron EDM,

$$d_e({\rm LXe}) < 6 \times 10^{-26}\, e \cdot {\rm cm}. \tag{63}$$

This projected limit is more than an order of magnitude worse than the present limit on the electron EDM from the Tl experiment [13], $d_e\,({\rm Tl}) < 1.6 \times 10^{-27}\, e \cdot {\rm cm}$. It is worth emphasizing that the above limit has been obtained using B-field sensitivity estimate from Ref. [44]; with the present sensitivity record [51], the constraints of electron EDM are

several orders of magnitude weaker. In other words, we find that a substantial improvement in the experimental sensitivity to weak magnetic fields is required before the CP-violating polarizability of liquid Xe can be used for EDM searches.

E. Conclusion

To summarize, we have computed novel T-violating atomic polarizabilities [46], $\beta^{\rm CP}$, for rare-gas atoms. We have derived third-order expressions for $\beta^{\rm CP}$ and employed the Dirac-Hartree-Fock method to evaluate the resulting expressions. We have elucidated the doubly relativistic origin of the polarizability and demonstrated strong Z^5 dependence on the nuclear charge. Finally, we evaluated a feasibility of setting a limit on the electron EDM by measuring T-violating magnetization of liquid Xe. We found that such an experiment could provide competitive bounds on electron EDM only if the present level of experimental sensitivity to ultra-weak magnetic fields [51] is improved by several orders of magnitude.

V. CONCLUSION

The intricate phenomenon of microscopic T-violation is viewed as a key to a deeper understanding of both the behavior of elementary particles and the matter-antimatter asymmetry of the Universe (see section I.A). T-violation has only been observed with certain kind of particles in accelerators. Very soon, in Geneva, the Large Hadron Collider (LHC) will replace the Large Electron Positron (LEP) collider. Physicists have a great expectation to finally reveal supersymmetry with the LHC. Experiments with atoms and molecules offer an alternative and complementary way to probe T-violation. They have already put tight constraints on elementary-particle models and, particulary, supersymmetry (see section I.B.3). At the same time, new atomic physics experiments might soon provide more answers to understanding the origin of the Universe and the laws that govern elementary particles. My dissertation provided a theoretical foundation for several emerging experimental searches for T-violation in atomic and molecular physics.

Here, using numerical estimates of structure factors, I related microscopic T-violating sources to macroscopic T-violating measurable signals. Three experiments were studied (Chapters II, III and IV). Each of them aims at measuring a T-violating signal in a sample of particular atoms or molecules. In some cases, the calculations were carried out for a number of species to find the best experimental candidate. In other cases, our work provides a guidance for searching better species and sets up techniques for future calculations of the relevant structure factors.

Let us sum up the results for the three considered experiments:

1) The conclusion of our work for the liquid Xe experiment (chapter II) is that experimentalists can expect an improvement of several orders of magnitude, compared to the present limit, for several sources of T-violation. Xenon atoms seem to be the best species for this experiment. This original work also develops computational techniques that can be used for atoms embedded in non-polar liquid. The results of this work were published in "Effects of confinement on the permanent electric-dipole moment of Xe atoms in liquid Xe", [54].

2) The purpose of the second experiment is to measure the electron EDM using trapped

molecular ions (chapter III). This experiment is planned at JILA, Colorado. We found that the considered molecular ions HBr^+ and HI^+ have structure factors lower than those for typical neutral molecules. The search for a better molecular ion candidate is still open. Our work provides a guideline for the search of a better molecular ion. This work was published in"Marked influence of the nature of chemical bond on CP-violating signature in molecular ions HBr^+ and HI^+", [55].

3) The third experiment (chapter IV) aims at putting a limit on the electron EDM by measuring the T-violating polarizability of liquid xenon. We found that such an experiment could provide competitive bounds on electron EDM only if the present level of experimental sensitivity to ultra-weak magnetic fields [51] is improved by several orders of magnitude. The idea of measuring a magnetic field produced by applying an electric field to a sample has not been abandoned though, and experimentalists and theoreticians are looking for other materials that would be much more sensitive to the electron EDM. It seems that molecules offer a better sensitivity again [56]. This work was published in "Atomic CP-violating polarizability", [57].

APPENDIX A: RELATIVISTIC ATOMIC ORBITALS

Non-relativistically, the wave function of an atomic electron is described by four quantum numbers: the principal quantum number (n), the angular momentum (l), the magnetic quantum number(m_l), and the projection of the spin (m_s). They correspond to the three degrees of freedom a point-like electron moving in a 3 dimensional space plus the one "internal" degree of freedom due to the orientation of the spin. The wave function of one electron is called an orbital. In a spherically symmetric potential it is usually denoted as $\varphi_{n,l,m}(\mathbf{r})$ or $\varphi_a(\mathbf{r})$, where a stands for the four quantum numbers. Spherical symmetry allows for factorization

$$\varphi_{n,l,m_l,m_s}(\mathbf{r}) = F_{n,l}(r)Y_{l,m_l}(\widehat{\mathbf{r}})\chi(m_s), \tag{A1}$$

where $Y_{l,m_l}(\widehat{\mathbf{r}})$ are the spherical harmonics and $F_{n,l}$ is the radial wave function.

Relativistically, the spin of the electron is coupled to the motion of the electron. The relativistic equation of motion of the electron is the Dirac equation. The spin degree of freedom is entangled to the three spatial degrees of freedom, and the total angular momentum $\mathbf{j} = \mathbf{l} + \mathbf{s}$ is introduced. For a spherically symmetric potential, the wave function of the electron is now described by three quantum numbers: the principal quantum number (n), the relativistic angular quantum number ($\kappa = (l - j)(2j + 1)$) and the magnetic quantum number (m). Sometimes the quantum number $j = |\kappa| - 1/2$ is used. The relativistic wave function of a single electron in a spherical potential is described by a bi-spinor (four complex numbers):

$$\varphi_a(\mathbf{r}) = \varphi_{n,\kappa,m}(\mathbf{r}) = \frac{1}{r}\begin{pmatrix} P_{n,\kappa}(r)\Omega_{\kappa,m}(\widehat{\mathbf{r}}) \\ iQ_{n,\kappa}(r)\Omega_{-\kappa,m}(\widehat{\mathbf{r}}) \end{pmatrix}, \tag{A2}$$

where P and Q are the radial wave functions for the small and large components, and $\Omega_{\kappa,m}(\widehat{\mathbf{r}})$ are the spherical spinors.

In independent-particle approximation, the atomic wavefunction of all electrons is repre-

sented by the Slater determinant of the occupied orbitals,

$$\Psi(\xi_1, \xi_2, ..., \xi_N) = \frac{1}{\sqrt{N!}} \begin{vmatrix} \varphi_1(\xi_1) & \varphi_2(\xi_1) & ... & \varphi_N(\xi_1) \\ \varphi_1(\xi_2) & \varphi_2(\xi_2) & ... & \varphi_N(\xi_2) \\ \vdots & \vdots & & \vdots \\ \varphi_1(\xi_N) & \varphi_2(\xi_N) & ... & \varphi_N(\xi_N) \end{vmatrix}, \tag{A3}$$

where a denotes a set of quantum numbers $n\kappa m$, N is the total number of electrons, and ξ_i encapsulates coordinate and spin degrees of freedom for the i^{th} electron. The determinant is needed in order to make the wavefunction antisymmetric, i.e., the wavefunction changes its sign when any two electrons are swaped (the Pauli principle for fermions).

APPENDIX B: HARTREE-FOCK APPROXIMATION

In the previous appendix, I introduced atomic orbitals by assuming that electrons move independently in a spherically-symmetric potential. This is an approximation, because interaction between the electrons generates a potential that depends on the position of all the electrons. This leads to an electronic wave function with correlations between the electrons. In the Hartree-Fock (HF) method, the wavefunction is approximated by a Slater determinant of electron orbitals, Eq.(A3). The radial wavefunctions P and Q, Eq.(A2), are determined using the variational principle. The variational principle gives solution to the wave equation,

$$(H - \varepsilon)\Psi = 0, \tag{B1}$$

by looking for the stationary solutions,

$$\langle \delta\Psi | H - \varepsilon | \Psi \rangle = 0. \tag{B2}$$

This equation leads to the Dirac-Hartree-Fock (DHF) equations for each orbital:

$$\left(c(\boldsymbol{\alpha} \cdot \mathbf{p}) + \beta c^2 + V_{\rm nuc} + V_{\rm HF} \right) \varphi_a = \varepsilon_a \varphi_a \,, \tag{B3}$$

where $V_{\rm HF}$ is a non-local self-consistent HF spherically symmetric potential and α's and β are the 4×4 Dirac matrices. Atomic units (Appendix C) were used. The DHF equations are solved self-consistently for the radial part of each orbital. The angular and spin part of each orbital $\Omega_{\kappa,m}(\widehat{\mathbf{r}})$ remains unchanged. At the end of the procedure the many-body atomic wavefunction Ψ is still written as a single Slater determinant of the orbitals. In more accurate theories (such as configuration interaction), a linear combination of Slater determinants is needed.

In our work we always started by solving DHF equations for occupied orbitals and excited (virtual) orbitals. It would give a complete basis of electron orbitals that we would use in all of our computations. To improve upon the DHF approximation, we also used relativistic random-phase approximation (RRPA) method [58]. This approximation describes a dynamic linear response of an atom to a perturbing one-body interaction (e.g., $H_{\rm CP}$). The perturbation modifies core orbitals thus changing the HF potential $V_{\rm HF}$. This modification

of V_{HF} in turn requires the orbitals to adjust self-consistently. Such a readjustment process defines an infinite series of many-body diagrams. The RRPA series can be summed to all orders using iterative techniques or solving DHF-like equations.

APPENDIX C: ATOMIC UNITS

In atomic physics, we employ a system of units called atomic units ($a.u.$). It is defined by taking the following basic quantities (in Gaussian units) equal to one $a.u.$:

- e is the absolute value of the electric charge of the electron,

- m is the rest mass of the electron,

- $\hbar$ is the Planck's constant divided by 2π.

All the other atomic units can be obtained by combining these quantities to give the proper dimension.

The first Bohr radius

$$a_0 = \frac{\hbar^2}{me^2} = 1a.u. \tag{C1}$$

is the atomic unit of length.

The fine-structure constant

$$\alpha = \frac{e^2}{c\hbar}, \tag{C2}$$

where c is the velocity of light in vacuum, is a pure number($\approx 1/137$). It means that

$$c \approx 137a.u. \tag{C3}$$

The atomic energy unit is

$$1H = \frac{me^4}{(4\pi\varepsilon_0)^2\hbar^2} = 1a.u. \approx 27.2eV. \tag{C4}$$

The Bohr magneton

$$\mu_B = \frac{e\hbar}{2m} \tag{C5}$$

has the value of $1/2$ in atomic units.

APPENDIX D: SOURCES OF T VIOLATION IN ATOMS

In this appendix, I compile sources of T-violation needed for my work. The Hamiltonians are written in the bi-spinor space (Appendix A).

1. Electron EDM

An electron has an EDM directed along its spin. Its value is d_e. The interaction of an electron EDM with an electric field $\boldsymbol{\mathcal{E}}$ has the form [12]:

$$H_e = 2d_e \begin{pmatrix} 0 & 0 \\ 0 & \boldsymbol{\sigma}\cdot\boldsymbol{\mathcal{E}} \end{pmatrix}, \tag{D1}$$

where σ's are the Pauli 2×2 matrices.

2. Nuclear Schiff moment

The Schiff moment S characterizes a difference between charge and EDM distributions inside the nucleus [16]. The Schiff moment is aligned with the nuclear spin $\mathbf{I}$:

$$\boldsymbol{S} = S\frac{\mathbf{I}}{\|\mathbf{I}\|}. \tag{D2}$$

The interaction between electrons and charges (and EDMs) conserves T. The Schiff moment originates from the T-odd interactions within the nucleus. The interaction of an electron with the nuclear Schiff moment has the form [24]

$$h_{\mathrm{SM}}(\mathbf{r}_e) = \frac{3}{B_4}\,\rho_N\left(\mathbf{r}_e\right)\left(\mathbf{r}_e\cdot\mathbf{S}\right), \tag{D3}$$

where ρ_N is the normalized nuclear density distribution and $B_4 = \int_0^\infty r^4\rho_N\left(r\right)dr$ is its fourth-order moment.

3. T-odd semileptonic interaction

The semileptonic interaction between the nucleus and the electron violates T and P. Its Hamiltonian may be represented as [22]

$$h_{\mathrm{TN}}(\mathbf{r}_e) = \sqrt{2} G_{\mathrm{F}}\, C_{\mathrm{TN}}\, \boldsymbol{\sigma}_N \cdot \left(i\gamma_0\gamma_5\, \boldsymbol{\sigma}\right)_e \rho_N\left(\mathbf{r}_e\right) \,. \tag{D4}$$

The subscripts e and N distinguish between operators acting in the space of electronic and nuclear coordinates, respectively. C_{TN} is the semi-leptonic coupling constant that characterizes the strength of this interaction, $G_{\mathrm{F}} = 2.2225 \times 10^{-14}$ a.u. is the Fermi constant, ρ_N is the normalized nuclear density distribution, and $\gamma_{0,5}$ are Dirac matrices.

4. T-odd weak neutral current

Recently there was a renewed interest to T-odd weak neutral current interactions of electrons with nucleons [59]. It is known that in atomic experiments, EDM of the electron is indistinguishable from the scalar T-odd weak neutral currents [49]. The interaction is represented as

$$h_{\mathrm{NC}}(\mathbf{r}_e) = \mathrm{i}\frac{G_{\mathrm{F}}}{\sqrt{2}}(Zk_1^p + Nk_1^n)\gamma_0\gamma_5\rho(\mathbf{r}_e) \equiv \mathrm{i}\frac{G_{\mathrm{F}}Z}{\sqrt{2}}K\gamma_0\gamma_5\rho(\mathbf{r}_e), \tag{D5}$$

where $k_1^{p,n}$ are dimensionless constants of the scalar P,T-odd weak neutral currents for proton and neutron ($K \equiv k_1^p + \frac{N}{Z}k_1^n$). Further, Z and N are the numbers of protons and neutrons in the nucleus, $\gamma_{0,5}$ are the Dirac matrices, and $\rho(\mathbf{r}_e)$ is the normalized nuclear density.

APPENDIX E: REDUCED MATRIX ELEMENTS

We use the Dirac bi-spinor introduced in Appendix A. The reduced matrix elements of the magnetic-dipole and electric-dipole moment operators between two bi-spinors are given by

$$\begin{aligned} \langle a||\mu||b\rangle &= \frac{1}{2}\left(\kappa_a+\kappa_b\right)\,\langle -\kappa_a||C_1||\kappa_b\rangle\,\times \\ &\quad \int_0^\infty r\;dr\{P_a\left(r\right)Q_b\left(r\right)+Q_a\left(r\right)P_b\left(r\right)\}\,, \end{aligned} \tag{E1}$$

$$\begin{aligned} \langle a||D||b\rangle &= -\langle \kappa_a||C_1||\kappa_b\rangle\,\times \\ &\quad \int_0^\infty r\;dr\{P_a\left(r\right)P_b\left(r\right)+Q_a\left(r\right)Q_b\left(r\right)\}\,, \end{aligned} \tag{E2}$$

$C_1(\hat{r})$ being the normalized spherical harmonic. For example, the matrix element of the electron EDM interaction Eq.(D1) reduces to

$$V_{ab}^{\mathrm{CP,EDM}} = d_e\left\{2Z\int_0^\infty \frac{dr}{r^2}Q_a\left(r\right)Q_b\left(r\right)\right\}\delta_{\kappa_a,-\kappa_b}\delta_{m_a,m_b}\,. \tag{E3}$$

We assumed that the dominant contribution is accumulated close to the nucleus (of charge Z) so that $\mathcal{E}$ can be approximated by the nuclear field. The selection rules with respect to angular quantum numbers m and κ arise because V^{CP} is a pseudoscalar.

APPENDIX F: DERIVATION OF EQ.(31)

Here I evaluate the sum (28) using the DHF approximation. The perturbation D_z, acting on Φ_0, induces two classes of intermediate states: (i) transfer of the hole g into some other state a and (ii) particle-hole excitations:

$$\begin{aligned} D_z|\Phi_0\rangle &= D_z a_g|0_c\rangle \\ &= -\sum_a \langle g|D_z|a\rangle a_a|0_c\rangle + \sum_{r,a}\langle r|D_z|a\rangle a_r^+ a_a a_g|0_c\rangle. \end{aligned}$$

$\langle\Phi_0|H_e$ is obtained by taking the Hermitian conjugate of the last expression and replacing D_z by H_e. Then we may express W_d as

$$\begin{aligned} W_d &= \frac{2}{R_e^2}\sum_{a\neq g}\langle a|H_e|g\rangle\frac{1}{\varepsilon_a-\varepsilon_g}\langle g|D_z|a\rangle + \\ &\frac{2}{R_e^2}\sum_{r,a}\langle a|H_e|r\rangle(\langle 0_c|a_g^+ a_a^+ a_a a_g|0_c\rangle)^2\frac{1}{\varepsilon_a-\varepsilon_r}\langle r|D_z|a\rangle. \end{aligned}$$

In the second term of the last expression, one has to take special care of the case $a = g$

$$\langle 0_c|a_g^+ a_a^+ a_a a_g|0_c\rangle = 1-\delta_{a,g},$$

leading to

$$\begin{aligned} W_d &= \frac{2}{R_e^2}\sum_{a\neq g}\langle a|H_e|g\rangle\frac{1}{\varepsilon_a-\varepsilon_g}\langle g|D_z|a\rangle \\ &- \frac{2}{R_e^2}\sum_{r}\langle g|H_e|r\rangle\frac{1}{\varepsilon_g-\varepsilon_r}\langle r|D_z|g\rangle \\ &+ \frac{2}{R_e^2}\sum_{r,a}\langle a|H_e|r\rangle\frac{1}{\varepsilon_a-\varepsilon_r}\langle r|D_z|a\rangle. \end{aligned}$$

The last term, containing summation over closed shell orbitals, vanishes as a result of the angular reduction. The non-zero contributions are

$$W_d = \frac{2}{R_e^2}\sum_{a\neq g}\frac{\langle g|D_z|a\rangle\langle a|H_e|g\rangle}{\varepsilon_a-\varepsilon_g} + \frac{2}{R_e^2}\sum_{r}\frac{\langle g|D_z|r\rangle\langle r|H_e|g\rangle}{\varepsilon_r-\varepsilon_g}, \tag{F1}$$

which is the Eq.(31) of the main text.

APPENDIX G: DERIVATION OF EQ.(32)

Here I will reduce the expression for W_d (31) to the Eq.(32). First we rewrite Eq.(31)

$$W_d = \frac{2}{R_e^2} \sum_{p \neq g} \frac{\langle g|D_z|p\rangle\langle p|H_e|g\rangle}{\varepsilon_p - \varepsilon_g}\,, \tag{G1}$$

where $p = \{n_p, \kappa_p, m_p\}$ denotes both core and virtual orbitals.

Let's first simplify the matrix element of the Hamiltonian H_e. Using the Wigner-Eckart theorem, one obtains

$$\langle p|H_e|g\rangle = 2d_e\delta_{\kappa_p,-\kappa_g}(-1)^{j_p-m_p} \begin{pmatrix} j_p & 0 & j_g \\ -m_p & 0 & m_g \end{pmatrix} \sqrt{2j_p+1} \times R_{EDM}\,,$$

with

$$R_{EDM} = -\int_0^\infty \mathcal{E}(r)Q_p(r)Q_g(r)dr. \tag{G2}$$

Selection rules on κ can also be written as

$$\delta_{\kappa_p,-\kappa_g} = \delta_{j_p,j_g}\delta_{l_p,2j_g-l_g}\,. \tag{G3}$$

Noticing that:

$$(-1)^{j_p-m_p} \begin{pmatrix} j_p & 0 & j_g \\ -m_p & 0 & m_g \end{pmatrix} \times \sqrt{2j_p+1} = \delta_{m_p,m_g}\,, \tag{G4}$$

one can simplify the matrix element:

$$\langle p|H_e|g\rangle = 2d_e\delta_{\kappa_p,-\kappa_g}\delta_{m_p,m_g}R_{EDM}\,. \tag{G5}$$

The summation over n_p, κ_p and m_p in (B1) is now reduced to a summation over just one quantum number, n_p. If the hole g is in a $p_{3/2}$ orbital ($\Pi_{3/2}$ molecule) then the summation is over all $d_{3/2}$ orbitals. If the hole g is in a $p_{1/2}$ orbital ($\Pi_{1/2}$ molecule) then the summation is over all $s_{1/2}$ orbitals.

Now let's simplify the matrix element of the electric dipole operator

$$\langle g|D_z|p\rangle = (-1)^{j_g-m_g} \begin{pmatrix} j_g & 1 & j_p \\ -m_g & 0 & m_p \end{pmatrix} \langle j_g||C^1||j_p\rangle \times R_D\,,$$

with

$$R_D = \int_0^\infty \left(f_p(r)f_g(r) + g_p(r)g_g(r)\right) r dr. \tag{G6}$$

EDM factor W_d can now be written

$$W_d = \frac{4d_e}{R_e^2} \sum_p \frac{(-1)^{j_g - m_g}}{\varepsilon_p - \varepsilon_g} \begin{pmatrix} j_g & 1 & j_p \\ -m_g & 0 & m_p \end{pmatrix} \langle j_g || C^1 || j_p \rangle \, R_D \, R_{EDM}.$$

This concludes the derivation of Eq.(32) of the main text.

[1] T. D. Lee, *Particle Physics and Introduction to Field Theory* (Harwood academic, Chur, Switzerland, 1981).

[2] E. Noether, Transport Theory and Statistical Physics **1**, 3 (1918).

[3] T. D. Lee and C. N. Yang, Phys. Rev. **104**, 254 (1956).

[4] C. S. Wu, E. Ambler, R. W. Hayward, D. D. Hoppes, and R. P. Hudson, Phys. Rev. **105**, 1413 (1957).

[5] T. D. Lee, R. Oehme, and C. N. Yang, Phys. Rev. **106**, 340 (1957).

[6] J. H. Christenson, J. W. Cronin, V. Fitch, and R. Turlay, Phys. Rev. Lett. **13**, 138 (1964).

[7] B. Aubert et al., Phys. Rev. Lett. **87**, 091801 (2001).

[8] L. M. Borkov and M. Zolotorev, Rep. Prog. Phys. **60**, 1351 (1997).

[9] A. D. Sakharov, Sov. Phys. JETP Lett. **5**, 24 (1967).

[10] L. D. Landau, Sov. Phys. JETP **5**, 405 (1957).

[11] N. Fortson, P. Sandars, and S. Barr, Physics Today **56**, 33 (2003).

[12] I. B. Khriplovich and S. K. Lamoreaux, *CP violation without strangeness. Electric dipole moments of particles, atoms, and molecules.* (Springer, Berlin, 1997).

[13] B. C. Regan, E. D. Commins, C. J. Schmidt, and D. DeMille, Phys.Rev.Lett. **88**, 071805 (2002).

[14] S. M. Barr and A. Zee, Phys. Rev. Lett. **65**, 21 (1990).

[15] J. M. Pendlebury and E. A. Hinds, N.I.M.P.R. **A 440**, 471 (2000).

[16] L. I. Schiff, Phys. Rev. **132**, 2194 (1963).

[17] M. V. Romalis and M. P. Ledbetter, Phys. Rev. Lett. **87**, 067601 (2001).

[18] R. Stutz and E. Cornell, Bull. Amer. Phys. Soc. **49**, 76 (2004).

[19] M. V. Romalis, W. C. Griffith, J. P. Jacobs, and E. N. Fortson, Phys. Rev. Lett. **86**, 2505 (2001).

[20] M. A. Rosenberry and T. E. Chupp, Phys. Rev. Lett. **86**, 22 (2001).

[21] V. L. Varentsov, V. G. Gorshkov, V. F. Ezhov, M. G. Kozlov, L. N. Labzovskii, and V. N.

Fomichev, Pis'ma Zh. Eksp. Teor. Fiz. **36**, 141 (1982), [JETP Lett. **36** 175 (1982)].

[22] A. Mårtensson-Pendrill, Phys. Rev. Lett. **54**, 1153 (1985).

[23] V. Dzuba, V. Flambaum, J. Ginges, and M. Kozlov, Phys. Rev. A **66**, 012111/1 (2002).

[24] V. Flambaum and J. Ginges, Phys. Rev. A **65**, 032113 (2002).

[25] S. H. Patil, J. Phys. B **35**, 255 (2002).

[26] P. Stampfli and K. H. Bennemann, Phys. Rev. A **44**, 8210 (1991).

[27] S. W.R.Johnson and J.Sapirstein, Phys.Rev. A **37**, 307 (1988).

[28] P.G.H.Sandars, Phys.Rev.Lett. **19**, 1396 (1967).

[29] J. J. Hudson, B. E. Sauer, M. R. Tarbutt, and E. A. Hinds, Phys. Rev. Lett. **89**, 023003 (pages 4) (2002).

[30] D. Wilkening, N. Ramsey, and D. Larson, Phys. Rev. A **29**, 425 (1984).

[31] J. Schropp, D., D. Cho, T. Vold, and E. Hinds, Rev. Lett.Phys. **59**, 991 (31 Aug. 1987).

[32] D. Cho, K. Sangster, and E. Hinds, Phys. Rev. Lett. **63**, 2559 (4 Dec. 1989).

[33] D. Kawall, F. Bay, S. Bickman, Y. Jiang, and D. DeMille, Phys. Rev. Lett. **92**, 133007 (2004).

[34] F. A.Chanda, W.C.Ho and I.Ozier, J.Mol.Spect. **169**, 108 (1995).

[35] F. A.Chanda, W.C.Ho and I.Ozier, J.Chem.Phys. **102**, 8725 (1995).

[36] H. Lefebvre-Brion and R. W. Field, *Perturbations in the spectra of diatomic molecules* (Academic Press, Orlando, 1986).

[37] M. G. Kozlov and D. DeMille, Phys. Rev. Lett. **89**, 133001 (pages 4) (2002).

[38] M. G. Kozlov and L. N. Labzowsky, J. Phys. B **28**, 1933 (1995).

[39] A. Dalgarno and J. T. Lewis, Proc. Roy. Soc. **223**, 70 (1955).

[40] M. G. Kozlov, J. Phys. B **30**, L607 (1997).

[41] Y. Takasu, K. Maki, K. Komori, T. Takano, K. Honda, M. Kumakura, T. Yabuzaki, and Y. Takahashi, Phys. Rev. Lett. **91**, 040404 (2003).

[42] F. L. Shapiro, Sov. Phys. Uspekhi **11**, 345 (1968), translation of Uspekhi Fizicheskii Nauk, vol.95, no.1, May 1968, p. 145-58.

[43] B. V. Vasil'ev and E. V. Kolycheva, Soviet Physics - JETP **47**, 243 (1978).

[44] S. K. Lamoreaux, Phys. Rev. A **66**, 022109 (2002).

[45] L. R. Hunter (2001), talk given at ITAMP workshop.

[46] V. G. Baryshevsky, Phys. Rev. Lett. **93**, 043003 (2004).

[47] P. G. H. Sandars, Phys. Lett. **14**, 194 (1965).

[48] L. D. Landau and E. M. Lifshitz, *Quantum Mechanics*, vol. III (Butterworth-Heinemann, 1997), 3rd ed.

[49] I. B. Khriplovich, *Parity non-conservation in atomic phenomena* (Gordon and Breach, New York, 1991).

[50] Amagat density unit is equal to 44.615 moles per cubic meter (mol/m^3).

[51] I. K. Kominis, T. W. Kornack, J. C. Allred, and M. V. Romalis, Nature **422**, 596 (2003).

[52] M. Romalis, private communications.

[53] D. Budker, D. F. Kimball, S. M. Rochester, V. V. Yashchuk, and M. Zolotorev, Phys. Rev. A **62**, 043403 (2000).

[54] B. Ravaine and A. Derevianko, Phys. Rev. A **69**, 050101(R) (2004).

[55] B. Ravaine, S. Porsev, and A. Derevianko, Phys. Rev. Lett. **94**, 013001 (2005).

[56] M. Kozlov and A. Derevianko, Phys. Rev. Lett. **97**, 063001 (2006).

[57] B. Ravaine, M. Kozlov, and A. Derevianko, Phys. Rev. A **72**, 012101 (2005).

[58] A. L. Fetter and J. D. Walecka, *Quantum Theory of Many-particle Systems* (McGraw-Hill, New York, 1971).

[59] K. P. Jungmann, Nucl. Phys. **A751**, 87 (2005).